POLSTRACC

Hermann Oelhaf, Björn-Martin Sinnhuber, Wolfgang Woiwode, Harald Bönisch, Heiko Bozem, Andreas Engel, Andreas Fix, Felix Friedl-Vallon, Jens-Uwe Grooß, Peter Hoor, Sören Johansson, Tina Jurkat-Witschas, Stefan Kaufmann, Martina Krämer, Jens Krause, Erik Kretschmer, Dominique Lörks, Andreas Marsing, Johannes Orphal, Klaus Pfeilsticker, Michael Pitts, Lamont Poole, Peter Preusse, Markus Rapp, Martin Riese, Christian Rolf, Jörn Ungermann, Christiane Voigt, C. Michael Volk, Martin Wirth, Andreas Zahn, and Helmut Ziereis

The POLSTRACC mission provided a wealth of data on the structure and composition of the Arctic lowermost stratosphere and upper troposphere during the extraordinarily cold winter 2015/16.

View from the research aircraft HALO on its way toward the North Pole: night sky above the Norwegian sea with aurora curtains and low level clouds above illuminated coastal areas (Photo by Tina Jurkat-Witschas).

Airborne Experiment for Studying the Polar Stratosphere in a Changing Climate with the High Altitude and Long Range Research Aircraft (HALO)

The Polar Stratosphere in a Changing Climate (POLSTRACC) campaign was the first comprehensive aircraft mission focusing on the Arctic lowermost stratosphere (LMS) over a whole winter–spring season. Changes of radiatively active trace gases such as ozone and water vapor in the lowermost stratosphere have a relatively large impact on climate forcing (e.g., Riese et al. 2012, and references therein). The coupling of the stratosphere with surface weather and climate has received considerable attention in recent years (e.g., Kidston et al. 2015, and references therein). The Arctic is the region with the largest observed climate change in the last decades (known as Arctic amplification; IPCC 2013). Yet, little is known of how climate change will affect chemical composition and processes in the Arctic stratosphere and how the feedback on surface climate will be.

After the discovery of the Antarctic ozone hole by Farman et al. (1985), the question was raised if comparable ozone depletion could also take place over the Arctic. Indeed, during cold stratospheric Arctic winters, substantial ozone depletion was observed ▶

also over the Arctic (e.g., Sinnhuber et al. 2000; Rex et al. 2004; Sinnhuber et al. 2011; WMO 2018), approaching in individual years losses that are comparable to the losses observed in the Antarctic (Manney et al. 2011). Weber et al. (2003) have shown that the interannual variability of high-latitude springtime total ozone columns over both hemispheres are quantitatively controlled by the activity of planetary-scale waves entering the stratosphere. Exceptional ozone columns such as in the disturbed Antarctic winter–spring of 2002 (Sinnhuber et al. 2003) or in the unusually cold Arctic winter–spring of 2010/11 (Sinnhuber et al. 2011) can be understood by exceptional wave activity in these winters.

Cold conditions in the winter polar stratosphere enable the formation of polar stratospheric clouds (PSCs) that serve as surfaces for heterogeneous chemical reactions, which are activating chlorine from the chemical less reactive reservoir compounds hydrochloric acid (HCl) and chlorine nitrate ($ClONO_2$) into reactive ClOx (=Cl + ClO + Cl_2O_2). ClOx can very efficiently destroy ozone in catalytic cycles once sunlight is available. Polar stratospheric clouds also heterogeneously convert nitrogen oxides (NO_x) into nitric acid (HNO_3), inhibiting the deactivation of ClO_x into chlorine nitrate (sometimes called denoxification). If polar stratospheric cloud particles can grow large enough to sediment efficiently, the nitric acid taken up in or on the PSC particles will be removed irreversibly from parts of the lower stratosphere (so-called denitrification), so that the halogen catalyzed ozone destruction can proceed even if temperatures are not cold enough for ongoing chlorine activation (Waibel et al. 1999; Fahey et al. 2001).

Heterogeneous chlorine activation can also take place on cold liquid aerosols, becoming efficient at temperatures below about 195 K (e.g., Drdla and Müller 2012). At temperatures below about 192 K sulfuric acid aerosol particles can efficiently take up HNO_3 so that they can grow considerably in size, becoming supercooled ternary ($H_2O/H_2SO_4/HNO_3$) solution (STS) polar stratospheric cloud particles (Carslaw et al. 1997; Schreiner et al. 1999). They are supercooled, because they coexist at temperatures below about 196 K with thermodynamically favorable nitric acid trihydrate (NAT) solid PSC particles. At temperatures below about 188 K, ice particles can form (Voigt et al. 2000a). At temperatures a few kelvins above the ice frost point T_{ice} (Murphy and Koop 2005), PSCs consisting of solid nitric acid trihydrate particles (NAT), STS droplets, and their mixtures can form, as shown by mass spectrometric composition measurements (Schreiner et al. 1999; Voigt et al. 2000a,b, 2005). While the role of the different PSC particles for chlorine activation is of secondary importance (Kirner et al. 2015), sedimentation of the larger NAT and ice particles becomes important for the irreversible redistribution of nitrogen compounds (denitrification and renitrification; Fahey et al. 2001).

Despite many similarities between ozone losses in cold Arctic winters and the Antarctic ozone hole, there are also fundamental differences (Solomon et al. 2014). In particular, although the degree of the ozone loss may be comparable in certain years, the actual amount of ozone in the Arctic is always larger than in the Antarctic ozone hole.

The connection between polar stratospheric ozone depletion and climate change is twofold, concerning

AFFILIATIONS: Oelhaf, Sinnhuber, Woiwode, Bönisch, Friedl-Vallon, Johansson, Kretschmer, Orphal, and Zahn—Institute of Meteorology and Climate Research, Karlsruhe Institute of Technology, Eggenstein-Leopoldshafen, Germany; Bozem, Hoor, and Krause*—Institute of Atmospheric Physics, University of Mainz, Mainz, Germany; Engel—Institute for Atmospheric and Environmental Sciences, Goethe University Frankfurt, Frankfurt, Germany; Fix, Jurkat-Witschas, Kaufmann, Marsing, Rapp, Wirth, and Ziereis—Institute of Atmospheric Physics, German Aerospace Center (DLR), Oberpfaffenhofen-Wessling, Germany; Grooß, Krämer, Preusse, Riese, Rolf, and Ungermann—Institute of Energy and Climate Research (IEK7), Forschungszentrum Jülich, Jülich, Germany; Lörks and Pfeilsticker—Institute of Environmental Physics, University of Heidelberg, Heidelberg, Germany; Pitts—NASA Langley Research Center, Hampton, Virginia; Poole—Science Systems and Applications, Inc., Hampton, Virginia; Voigt—Institute of Atmospheric Physics, German Aerospace Center (DLR), Oberpfaffenhofen-Wessling, and Institute of Atmospheric Physics, University of Mainz, Mainz, Germany; Volk—Institute for Atmospheric and Environmental Research, University of Wuppertal, Wuppertal, Germany
* **CURRENT AFFILIATION:** Excelitas Technologies GmbH and Co. KG, Wiesbaden, Germany
CORRESPONDING AUTHORS: Hermann Oelhaf, hermann.oelhaf@kit.edu; Björn-Martin Sinnhuber, bjoern-martin.sinnhuber@kit.edu

The abstract for this article can be found in this issue, following the table of contents.
DOI:10.1175/BAMS-D-18-0181.1

A supplement to this article is available online (10.1175/BAMS-D-18-0181.2)

In final form 25 July 2019

the following questions: 1) How will climate change due to the anthropogenic emission of greenhouse gases affect the polar winter stratosphere? 2) What is the impact of changes in the polar stratosphere on surface climate?

Overall, the stratosphere is cooling in response to the increase in greenhouse gases (Goessling and Bathiany 2016). This is clearly seen in the middle and upper stratosphere. Climate models project a further cooling. However, climate models also project an increase in the strength of the large-scale meridional Brewer–Dobson circulation that would lead to a warming of the polar lower stratosphere (WMO 2018, and references therein). This has led to the notion, that the cold, undisturbed, Arctic stratospheric winters may be getting colder while overall there may be no clear trend or even a warming (Rex et al. 2004; Sinnhuber et al. 2011; Bohlinger et al. 2014). In spite of these factors, the Arctic winter lower stratosphere experiences new record low temperatures roughly every 5 years since the early 1990s. However, whether there is robust statistical evidence remains an open topic (e.g., Rieder and Polvani 2013).

There is now clear evidence that the Antarctic ozone hole has significantly affected surface climate change on the Southern Hemisphere (e.g., Thompson et al. 2011; WMO 2018). Ozone depletion in the Antarctic ozone hole has resulted in a cooling of the stratosphere between late winter and early summer, resulting in a poleward shift of the westerly winds that propagate down to the surface. This in turn leads to changes in rainfall and weather patterns. For the Arctic, however, the situation is much less clear. Although in individual Arctic winters the amount of ozone chemically depleted approaches that in the Antarctic ozone hole (e.g., Manney et al. 2011), the loss is generally smaller than in the Antarctic, the polar vortex does not persist as long into spring when solar radiation becomes important, and the large interannual variability in the Arctic makes detection and attribution more difficult. More recently, a number of studies have provided evidence that Arctic ozone changes can impact surface climate (Smith and Polvani 2014; Calvo et al. 2015; Ivy et al. 2017).

Little focus has so far been placed on the lowermost Arctic stratosphere, say below 100-hPa pressure altitude. The majority of the column integrated chemical ozone depletion in the Arctic takes place between approximately 17- and about 25-km altitude (e.g., WMO 2018), but much less is known about the upper troposphere–lowermost stratosphere (UTLMS) region where trace gas changes have a relatively large radiative effect for surface climate forcing (e.g., Riese et al. 2012). There is still large uncertainty of the expected ozone recovery in the extratropical and high-latitude UTLMS and the associated radiative forcing (Bekki et al. 2013). The polar vortex is less well defined in the LMS below about 100-hPa pressure altitude, and chemical ozone changes are more difficult to quantify at these altitudes. Moreover, satellite observations of trace gases often have limited precision and accuracy in the UTLMS region, so that our understanding of the chemical and transport processes in this altitude region is incomplete (Hegglin et al. 2013). Nevertheless, there is evidence for chlorine activation and resulting chemical ozone depletion also in the lowermost Arctic (and Antarctic) stratosphere from satellite observations (e.g., Santee et al. 2011). Short-lived halogen compounds, predominantly from natural sources, can have a relatively large impact on ozone depletion in the polar lowermost stratosphere (Hossaini et al. 2015; Sinnhuber and Meul 2015; Fernandez et al. 2017), but these processes are still not well represented in current chemistry climate models.

THE POLSTRACC MISSION: OBJECTIVES AND MAIN ACTIVITIES. *Scientific objectives.* To address remaining questions on chemistry and transport processes in the Arctic upper troposphere–*lowermost* stratosphere under the present load of ozone-depleting substances and state of climate variables, the POLSTRACC campaign was conducted in the Arctic winter 2015/16, several years after past intensive Arctic campaigns [e.g., SOLVE/THESEO-2000 in 1999/2000 (Newman et al. 2002), EUPLEX/SOLVE-II in 2002/03, RECONCILE in 2009/10 (von Hobe et al. 2013)]. By deploying the German High Altitude and Long Range Research Aircraft (HALO), POLSTRACC was designed to study the Arctic UTLMS along with its coupling with lower latitudes throughout an entire winter–spring cycle, with the following specific scientific objectives (see also Fig. 1):

1) investigate the structure, composition, and dynamics of the bottom of the polar vortex and its coupling with the upper troposphere and extravortex air masses, to quantify transport and mixing, and to identify the role of special events such as tropopause folds and polar lows;
2) study polar stratospheric clouds and high-altitude cirrus in the UTLMS in Arctic winter and spring;
3) examine the vertical redistribution of HNO_3 by PSCs and underlying processes;

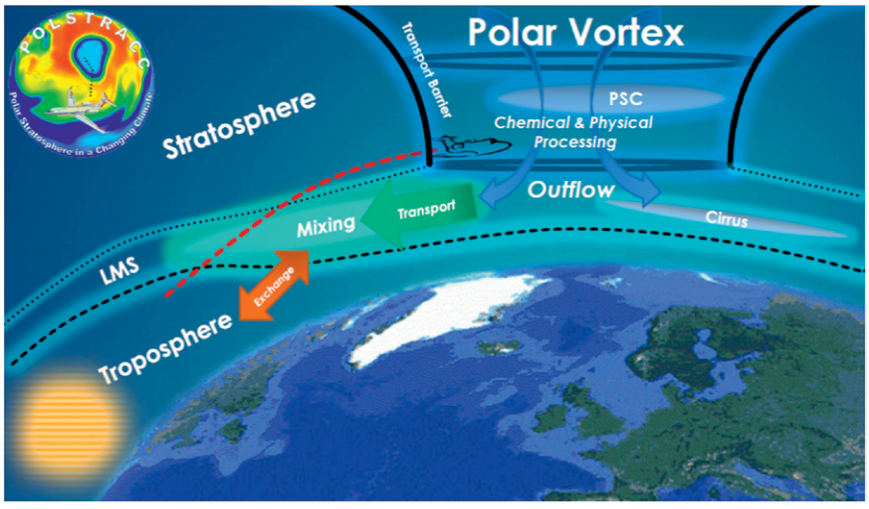

Fig. 1. POLSTRACC focused on the winter–spring Arctic LMS, its underlying processes, and its linkages to middle latitudes and the upper troposphere. Processed air from the polar vortex outflow can be transported rapidly toward lower latitudes with an impact on local chemistry and radiative budgets.

4) investigate chlorine activation/deactivation in the Arctic LMS and assess the role of bromine compounds; and
5) quantify ozone loss in the LMS.

Selected scientific highlights achieved from the mission data addressing these objectives are discussed in the section "Highlighted results."

Overall mission strategy. POLSTRACC was designed to cover the whole Arctic winter from the onset of the polar vortex in early winter until its breakdown in spring, utilizing the capabilities of HALO, requiring flight operations between December and March over a wide geographical area. HALO (www.halo.dlr.de/; www.halo-research.de) is a Gulfstream 550 twin-engine jet aircraft, with about 10,000-km range, up to 15-km ceiling altitude, and a payload capacity of about 3 tons. The POLSTRACC (www.polstracc.kit.edu/polstracc/img_auth.php/POLSTRACC_Whitebook_v2.4.2.pdf) payload consisted of a dedicated combination of in situ and remote sensing instrumentation providing highly resolved and accurate observations of the polar UTLMS region and making use of the synergy from parallel in situ and remote sensing measurements. A large suite of meteorological diagnostics and forecast tools along with Lagrangian chemistry-transport models driven by ECMWF forecasts was used for detailed flight planning.

The POLSTRACC campaign was arranged in three phases: 1) early winter: 17–21 December 2015, 2) midwinter: 12 January–2 February 2016, and 3) late winter–spring: 26 February–18 March 2016. During phases 2 and 3, HALO was operated mainly from Kiruna, Sweden (68°N, 20°E), while the early winter survey flights during phase 1 and the late winter surveys during phase 3 were conducted from HALO's home base at Oberpfaffenhofen, Germany (48°N, 11°E).

In total, 18 scientific flights adding up to 156 flight hours covered the time span from 17 December 2015 until 18 March 2016. The maximum ceiling level achieved was 14.6 km (FL480), the minimum air temperature was –76°C, and the maximum ranges with and without fuel stops were 9,332 and 8,060 km, respectively.

Synergies from combining the projects POLSTRACC, GW-LCYCLE, and SALSA to one joint campaign. The POLSTRACC mission was operated in close connection with two other projects dedicated to complementary science issues by sharing the same instrumentation and joining forces in several aspects: GW-LCYCLE (Gravity Wave Life Cycle Experiment) and SALSA (Seasonality of Air mass transport and origin in the Lowermost Stratosphere using HALO Aircraft). The usage of a shared payload, the same campaign base, and the same infrastructure considerably reduced the efforts of payload/aircraft certification, campaign logistics, and flight operations. The combination of the projects into one joint and focused campaign has extended the available datasets of the individual projects and therefore broadened their scientific scopes, enabling the study of the links between the processes that have been in the focus of the individual projects.

GW-LCYCLE (Wagner et al. 2017) addressed dynamical coupling processes by gravity waves from the troposphere into the mesosphere, with the goal to improve gravity wave parameterizations in climate models. GW-LCYCLE employed—in addition to HALO measurements—observations on board the Falcon 20-E research aircraft operated by Deutsches Zentrum für Luft- und Raumfahrt (DLR), ground-based observations, correlative satellite observations, and numerical modeling. Science issues dedicated to

GW-LCYCLE were embedded in the overall flight planning operated from Kiruna leading to six flights focusing on gravity wave science aspects (Dörnbrack et al. 2018), with a special focus on the tomographic capabilities of the Gimballed Limb Observer for Radiance Imaging of the Atmosphere (GLORIA) aboard HALO (Friedl-Vallon et al. 2014; Riese et al. 2014; Krisch et al. 2017). During the parallel deployment of HALO and Falcon at Kiruna during phase 1, coordinated flights of Falcon and HALO were realized.

The overall scientific rationale of SALSA (http://gepris.dfg.de/gepris/projekt/109259784) was to improve the understanding of UTLS transport and chemistry in the transition region between the subtropics and the Northern midlatitudes through a better knowledge of the seasonality of trace gas distributions. In conjunction with the POLSTRACC mission, a special focus was laid on the winter–spring season. For this purpose, several HALO flights were conducted to study intrusions of subtropical and midlatitude air to the Arctic. Along with two flights, dedicated to SALSA science, heading toward the subtropics at the begin and end of the whole joint mission, HALO was covering a much more extended latitudinal area (25°–87°N) than in previous Arctic aircraft campaigns.

HALO flights are coded here as "PGS-nn," reflecting the combination of POLSTRACC, GW-LCYCLE, and SALSA project goals, while the discussion of this paper only focuses on POLSTRACC science issues.

Table 1. Instruments aboard HALO during the POLSTRACC campaign.

Instrument	Primary target parameters	Technique	Institution	Primary references
GLORIA	O_3, HNO_3, H_2O, CFCs, $ClONO_2$, temperature	Imaging Fourier transform spectrometer (IFTS)	IMK-ASF, KIT; IEK-7, FZJ	Friedl-Vallon et al. (2014); Riese et al. (2014)
Mini-DOAS	O_3, NO_2, BrO, OClO	UV–VIS–NIR spectrometer	University of Heidelberg	Platt and Stutz (2008); Hüneke et al. (2017)
WALES	Aerosol, H_2O, O_3	Lidar	DLR-IPA	Wirth et al. (2009); Fix et al. (2019)
AENEAS	NO, NO_y, particulate NO_y	Chemiluminescence	DLR-IPA	Ziereis et al. (2000); Ziereis et al. (2004); Stratmann et al. (2016)
AIMS	HCl, HNO_3, $ClONO_2$, SO_2	Mass spectrometer	DLR-IPA	Jurkat et al. (2016); Voigt et al. (2014); Jurkat et al. (2017)
BAHAMAS	Meteorological and avionic data	Air data boom, inertial sensors, GNSS, video and A/C ARINC interface	DLR-FX	Krautstrunk and Giez (2012)
FAIRO	O_3	UV photometer/ chemiluminescence	IMK-ASF, KIT	Zahn et al. (2012)
FISH	Total and gas-phase H_2O	Lyman-Alpha hygrometer	IEK-7, FZJ	Zöger et al. (1999); Meyer et al. (2015)
GhOST-MS	CH_3Br, $CHBr_3$, $CHCl_3$, CH_3I, CFCs, SF_6	GC-MS	University of Frankfurt	Sala et al. (2014); Bönisch et al. (2011); Engel et al. (2006)
HAGAR-V	CO_2, SF_6, CH_4, N_2O, CFCs, chlorinated VSLS	NDIR, GC-ECD, GC-MS	University of Wuppertal	Werner et al. (2010)
HAI	Total and gas-phase H_2O	Tunable Diode Laser (TDL; closed and open path)	PTB	Buchholz et al. (2017)
Dropsonde	Pressure, temperature, humidity, wind	Dropsonde system	DLR-IPA	Voigt et al. (2017)
TRIHOP	CO, N_2O, CH_4 CO_2	QCL–IR absorption spectrometer	University of Mainz	Krause et al. (2018)
WARAN	Total and gas-phase H_2O	TDL spectrometer	DLR-IPA	Kaufmann et al. (2014, 2016, 2018)

Payload. POLSTRACC utilizes a combination of 10 in situ and three remote sensing instruments on HALO (Table 1; Fig. 2). This dedicated UTLS payload weighs about 3 tons. A similar payload had already been used before during the TACTS/ESMVAL mission in 2012 (Müller et al. 2016) and was later on used during the WISE mission in 2017 (www.wise2017.de/; Kunkel et al. 2019). Further deployment of this payload with minor modifications is used for studying the Southern Hemisphere mid- to high-latitude UTLS during the SOUTHTRAC mission recently operated in September and November 2019.

This payload exploits the synergy of local but highly specific and precise in situ observations at the aircraft location with 2D and 3D distributions of atmospheric parameters achieved from remote sensing instruments capable of adding information on the atmosphere above and/or below the aircraft. Dropsondes were released for specific case studies as well as validation, and for providing temperature, tropospheric humidity, and wind velocity. The overall payload is capable of measuring a large suite of parameters with respect to physical conditions (pressure, temperature, wind velocity, turbulence), chemical composition (trace gas composition), clouds (PSCs, cirrus clouds, and aerosol), and dynamic processes (using combinations of these parameters, in particular tracers of different lifetimes).

The three *remote sensing instruments* provided *vertical* distributions of selected parameters (particularly PSCs, aerosol, temperature, O_3, H_2O, NO_2, HNO_3, $ClONO_2$, OClO, BrO), *below* the aircraft by applying passive infrared limb imaging (GLORIA; Friedl-Vallon et al. 2014; Riese et al. 2014), and ultraviolet (UV)–visible (VIS)–near-infrared (NIR) differential optical absorption spectroscopy

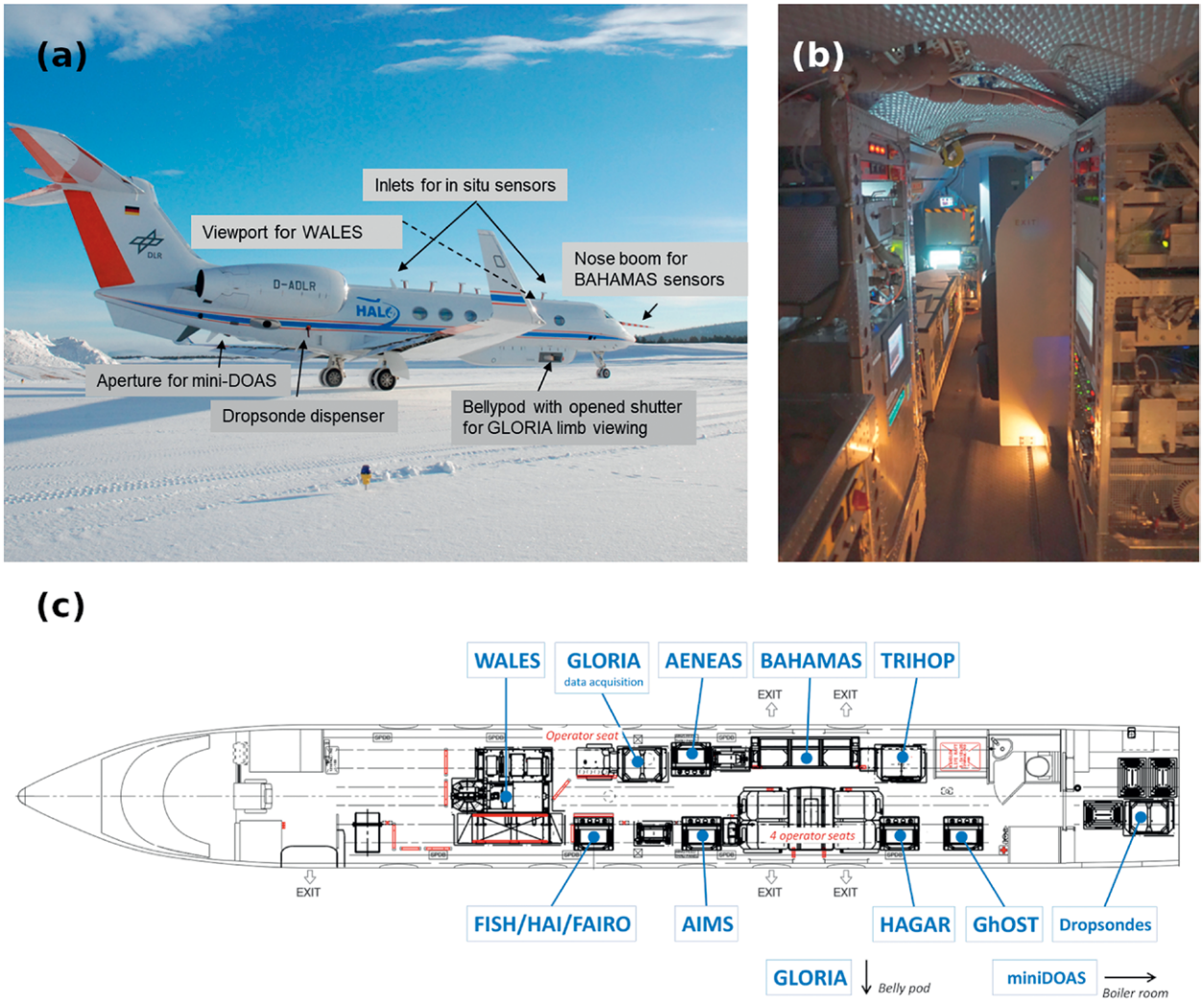

Fig. 2. (a) HALO in POLSTRACC configuration, (b) cabin view with POLSTRACC instrumentation, and (c) corresponding cabin layout.

(mini-DOAS; Hüneke et al. 2017), and *above* the aircraft using the new multiwavelength lidar system WALES (Wirth et al. 2009).

The 10 *in situ instruments* apply various techniques, including mass spectrometry (MS), gas chromatography (GC), chemiluminescence, and different spectroscopic techniques, allowing highly precise and time-resolved observations of a large number of avionic and meteorological data, O_3, gas phase and total H_2O, tracers of different lifetimes (CO_2, N_2O, CH_4, CO, SF_6, CFCs, NMHCs, halogens, bromine-containing VSLS, and others), chemically active species such as HNO_3, HCl, $ClONO_2$, NO, NO_y, and particulate NO_y and H_2O.

A detailed description of the payload can be found in the online supplemental material (https://doi.org/10.1175/BAMS-D-18-0181.2).

Related ground-based and satellite observations. Cooperation with ground-based observation stations, balloon sounding activities (ozone soundings and radiosondes), and satellite-borne projects [i.e., Cloud–Aerosol Lidar with Orthogonal Polarization (CALIOP; Pitts et al. 2018), Microwave Limb Sounder (MLS; Santee et al. 2011), Atmospheric Chemistry Experiment–Fourier Transform Spectrometer (ACE-FTS; Bernath et al. 2005)] were initiated and pursued to extend the scientific scope of POLSTRACC and for flight planning. Tight cooperation was realized with the CALIOP and MLS teams, both during the campaign and for data analysis. CALIOP science team members were present in Kiruna during the midwinter phase of the campaign and CALIOP data quick looks were regularly used for flight planning during the PSC season. One flight was realized for matching spaceborne CALIOP and airborne WALES PSC measurements. Both CALIOP and MLS data were later on used in a number of joint publications by POLSTRACC consortium members.

Data from ground-based stations in the European Arctic, particularly of the ground-based lidars in Kiruna (68°N, 20°E) and Andenes (69°N, 16°E) on the windward and leeward sides of the mountains, were embedded in the mission planning of the intensive observation periods and in scientific data exploitation. During midwinter, frequent radiosonde and balloon-borne lightweight hygrometers were launched from Kiruna Airport and Andenes. Ozone-lidar operations and ozone radiosondes launches from Ny-Ålesund/Spitsbergen (79°N, 12°E) were coordinated with HALO flight routes covering the Spitsbergen area.

Modeling activities. Modeling activities were used for flight planning of the POLSTRACC campaign and for postflight data analysis. In particular, the Chemical Lagrangian Model of the Stratosphere (CLaMS) and the chemistry climate model ECHAM–MESSy Atmospheric Chemistry (EMAC) were closely involved in POLSTRACC.

The chemistry transport model CLaMS is based on a Lagrangian formulation of tracer transport (McKenna et al. 2002; Konopka et al. 2004) and driven by ECMWF forecasts and reanalyses. CLaMS considers an ensemble of air parcels on a time-dependent irregular grid that is transported and mixed employing 3D trajectories. The model provides global and high resolution (up to 20-km horizontal resolution and a-few-hundred-meters vertical resolution) and covers both the troposphere and the stratosphere. CLaMS also includes a denitrification scheme including an implementation of nucleation, growth, and sedimentation of NAT particles that are transported on Lagrangian trajectories (Grooß et al. 2014, and references therein). The formation of cirrus clouds was simulated by the model system CLaMS-ice, in which a two-moment bulk cirrus scheme (Spichtinger and Gierens 2009) was coupled to CLaMS trajectories; in forecast mode this model system was used to predict areas of cirrus occurrence. CLaMS was used for flight planning and forecasting; for the analysis of photochemistry, transport, and mixing processes; for studies of PSCs and denitrification; and for analysis of the radiative budget. For postflight analysis of the results, a CLaMS simulation was performed using ERA-Interim (Dee et al. 2011), and satellite observations by MLS for initialization and boundary conditions (Grooß et al. 2018).

Simulations with the chemistry climate model EMAC complemented the CLaMS activities by providing a large-scale and long-term context and for investigating the climate impact of the investigated processes (Khosrawi et al. 2017). The chemistry climate model EMAC is based on the climate model ECHAM5 (fifth-generation European Centre Hamburg general circulation model) and the Modular Earth Submodel System (MESSy; Jöckel et al. 2010). EMAC is a global model, covering the atmosphere from the surface up to about 80-km altitude. EMAC was used in a version nudged with meteorological analyses or reanalyses (ECMWF operational and ERA-Interim) at T106 spectral truncation to support point-by-point comparisons with observations.

Further modeling activities in the POLSTRACC framework include high-resolution simulations of the UTLS on regional scale by the seamless chemistry–climate model ICON-ART (Schröter et al. 2018).

Campaign and flight management. The campaign was run from Oberpfaffenhofen at the beginning and end of the mission, and from Kiruna during midwinter–early spring. An interactive website (www.polstracc.kit.edu), based on the MediaWiki software, was set up as a living document platform, including up to date information of important aspects to keep all campaign participants on site and at remote locations informed.

A small core group consisting of the mission coordinators, meteorologists, modelers, and, on a case by case basis, other interested scientists regularly discussed and prepared possible flight plans on the basis of available data (MLS and CALIOP quick looks, ground-based observations, meteorological analyses) and CTM predictions of a series of forecast products. Detailed scientific flight planning made use of a dedicated Mission Support System (MSS) tool (Rautenhaus et al. 2012) that was extended and adapted to the POLSTRACC needs. Forecast products were based on ECMWF deterministic forecasts and chemical transport model forecasts with CLaMS (Grooß et al. 2014). More details and an example of the process of planning, implementation, execution, and reporting of science flights are given in the supplemental material.

Meteorological situation. The Arctic winter 2015/16 was extraordinary in the sense that in November–December 2015 the coldest and strongest Arctic polar vortex for almost 70 years formed (Matthias et al. 2016), setting the stage for the greatest potential yet seen for record Arctic ozone loss (Manney and Lawrence 2016). Synoptic PSCs formed over a long period of time in early winter, vertically extending down to altitudes lower than 15 km (Pitts et al. 2018; Voigt et al. 2018). Temperatures below the ice frost point were detected throughout January 2016 at 30 hPa (Dörnbrack et al. 2016). In February, three minor stratospheric warmings led to slightly warmer conditions in the polar vortex, with temperatures still below the NAT stability temperature T_{NAT} (Hanson and Mauersberger 1988). The final stratospheric warming started around 5 March 2016 (Manney and Lawrence 2016), which resulted in a split of the vortex, and ended the cold conditions. The exceptional coldness of the Arctic winter 2015/16 and its evolution with respect to the long-term climatology is illustrated in Fig. 3.

The cold conditions during POLSTRACC mission phases 1 and 2

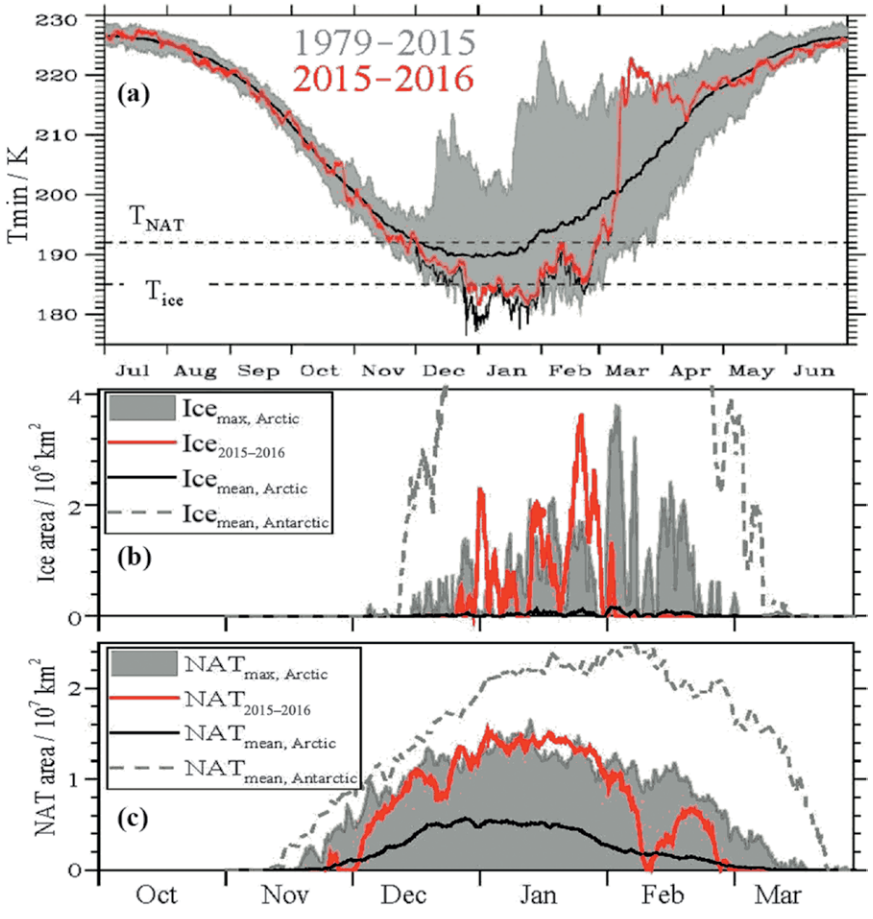

FIG. 3. Minimum temperatures and potential PSC existence areas in the 2015/16 winter from ECMWF analyses in comparison with previous winters. The red lines show the evolution of winter 2015/16 from ECMWF operational analyses, while the thick black lines and the gray shading show the mean and range over the 1979–2016 period from ERA-Interim. (a) Minimum temperatures north of 65°N. Horizontal dashed lines indicate the PSC existence temperatures for NAT (T_{NAT}) and ice (T_{ice}). The thin black line indicates results from a higher-resolution pre-operational analysis that becomes operational after 8 Mar 2016. (b) Area of temperatures below T_{ice}. (c) Area of temperatures below T_{NAT}. Dashed lines in (b) and (c) show Antarctic mean for comparison (shifted by 6 months). Adapted from Voigt et al. (2018), CC Attribution 4.0 License.

Table 2. Overview of PGS flights of phase 1 (early winter). Date, mission scope, target region, additional observations/remarks, and operational flight data are given (EDMO = Oberpfaffenhofen, Germany).

Flight No.	Date	Primary mission scope	Research topics	Target region	Additional observations/ remarks	Operational flight data
PGS-01 to PGS-03		Test flights	Instrument testing	Germany	Instrument certification, EMV and test flights	· Base: EDMO · Duration: short · Max flight level: various
PGS-04	17 Dec 2015	Survey flight	Access a wide range of equivalent latitude and $\Delta\theta$	Western Europe (40°–61°N, 0°–11°W)	SALSA-1 flight	· Base: EDMO · Duration: 8 h 30 min · Max flight level: FL 470
PGS-05	21 Dec 2015	Early vortex survey	Early vortex state and composition, filamentary stratospheric structures	Northern Europe, surrounding Spitsbergen (48°–81°N)	Coordinated with ground-based observations (including ozone sonde) at Ny-Ålesund, Spitsbergen	· Base: EDMO · Duration: 9 h 43 min · Max flight level: FL 460

provided ideal conditions to investigate PSC formation, redistribution of HNO_3, and chlorine activation. The major stratospheric warming during phase 3 allowed us to address in detail air mass exchange and mixing under these distorted conditions.

Overview of scientific flights. In total, 18 scientific flights were conducted in the time span from 17 December 2015 to 18 March 2016. Tables 2–4 present for every single flight of the three mission phases summaries of primary flight objectives and addressed research topics along with essential operational flight parameters.

A detailed description of the individual flights including maps of flight paths on maps of potential temperature is provided as a supplement to this paper.

Mission phase 1: Early winter. Two survey flights before the Christmas break were conducted from the home base at Oberpfaffenhofen to provide an overview of the state and composition of the UTLMS on long transects covering a wide range of latitudes (Table 2, Fig. 4). In PGS-04 the focus was put on the subtropical to middle latitudes dedicated to SALSA science objectives. PGS-05 was the first flight of POLSTRACC to the Arctic, probing the transition region between middle latitudes and the Arctic (48°–81°N), in a situation when the vortex had already cooled down to temperatures below PSC existence temperatures over large areas.

Mission phase 2: Midwinter. Eight flights between 12 January and 2 February 2016 (Table 3, Fig. 4) covered the midwinter period, that was characterized by a stable polar vortex and record-low stratospheric temperatures. Apart from the transfer flight PGS-06

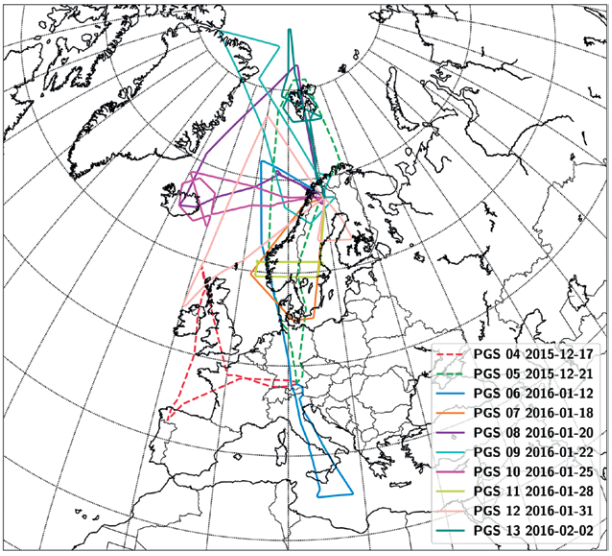

Fig. 4. Flight routes of phases 1 and 2: early winter flights (PGS-04 and PGS-05; dashed), transfer to Kiruna via Malta (PGS-06), and midwinter flights (PGS 07–13).

on 12 January, all flights were performed from Kiruna Airport (ENSQ). These flights were conducted in the coldest period of the winter with synoptic PSCs often occurring in the lowermost stratosphere down to the local tropopause (Fig. 5). A tropopause fold in connection with mountain wave activity sampled during PGS-06 was studied in detail by Woiwode et al. (2018) (see the "Highlighted results" section, Fig. 10). Enhanced HNO_3 at the bottom of the vortex was already detected by GLORIA on this flight which indicated nitrification of the LMS (Johansson et al. 2018; Braun et al. 2019). Further clear signs of

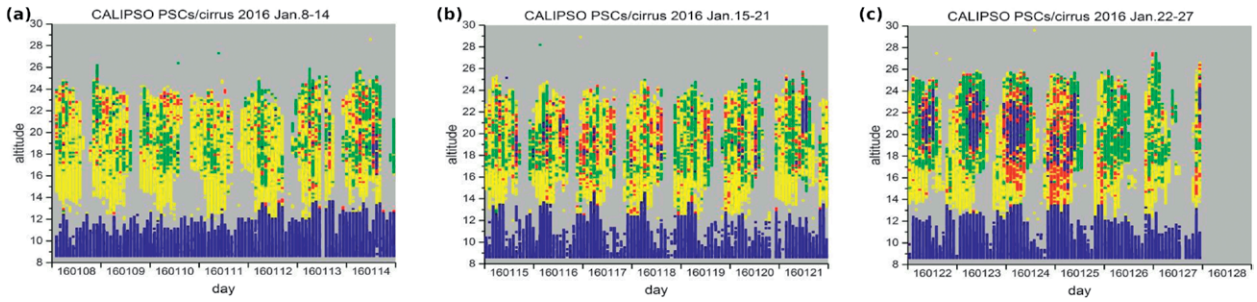

Fig. 5. Cloud occurrence for three weeks in January 2016. Vertical bars represent the altitude extent of cirrus (blue lower altitudes) and PSCs (color coded by composition: green, STS; yellow–red, mixed; blue in stratosphere, ice) observed by CALIOP along each of the ~15 orbits per day. PSCs frequently extended in altitude from the tropopause to 25-km altitude, which is more typical of the Antarctic than the Arctic. Ice clouds (blue colors) are found frequently between 20 and 25 Jan 2016.

renitrified and chlorine-activated air were found in filamented vortex air over Scandinavia in PGS-07. In situ instruments detected several layers of enhanced nitric acid at flight level (FL) 450 (45,000 ft; 1 ft ≈ 0.305 m). At the uppermost FL 470 sharp enhancements of particulate NO_y were measured by the NO_y channel of the forward facing inlet. PGS-08 was planned to probe air underneath the cold pool of the vortex and to study the extent and character of synoptic PSCs above the Norwegian Sea between Scandinavia, Iceland, and Spitsbergen with a turning point as far as 87°N. Evidence of ongoing nitrification of the Arctic LMS was observed by GLORIA, reaching up to 7 ppbv of gas-phase HNO_3, while particulate NO_y was detected from in situ measurements at flight altitude. PGS-09 was particularly devoted to the study of PSCs matching air masses of two overpasses of *CALIPSO* satellite tracks (Voigt et al. 2018; cf. Fig. 11 and Fig. 12 in the "Highlighted results" section). An exceptional finding during the POLSTRACC flights was the in situ detection of large HNO_3-containing particles at low stratospheric altitudes around 14 km by the Atmospheric Nitrogen Oxides Measuring System (AENEAS) instrument, as illustrated for PGS-10 in Fig. 13 in the "Highlighted results" section. PGS-12 went south to the northern tip of Ireland where a warm conveyor belt (WCB) pushed the tropopause height up to FL 450. A very strong jet stream was crossed twice by the flight pattern, from the Arctic stratosphere to subtropical air and on the way back to Kiruna (see supplemental material for more detail). On a section of the same flight observations at constant solar zenith angle (SZA) were arranged to investigate chlorine/bromine chemistry by DOAS UV–VIS–NIR observations (see Fig. 17 in the "Highlighted results" section).

Coordinated flights of Falcon and HALO aircrafts were conducted over Scandinavia during a mountain wave event (PGS-11). Particularly PGS-10 and PGS-13 were tailored to explore in detail gravity waves with HALO flights above Iceland and Spitsbergen, respectively, by making use of hexagon-like flight patterns in order to enable tomographic retrievals from GLORIA measurements (Ungermann et al. 2011; Krisch et al. 2017).

Mission phase 3: Late winter–spring. Eight flights between 26 February and 18 March covered the late winter period (Table 4, Fig. 6). The vortex started to shrink with the sudden major warming around 5–6 March (Manney and Lawrence 2016) followed by a vortex split and a displacement of the vortex far off the pole.

Three flights (PGS-14, PGS-17, PGS 19) were primarily devoted to access strongly subsided air masses

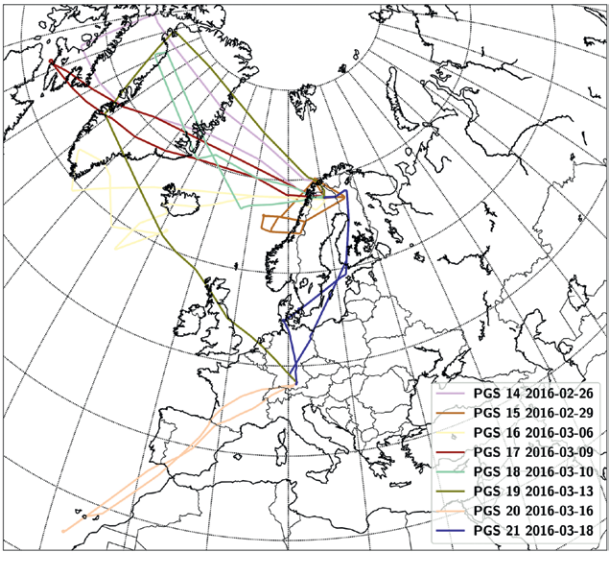

Fig. 6. Flight routes of phase 3: late winter–spring flights (PGS-14–18), transfer flight to the home base at Oberpfaffenhofen (PGS-19), and local flights from the home base (PGS-20–21).

between Greenland and Canada in order to characterize low N_2O, high DO_3, ClO_x, DNO_y, and $ClONO_2$ at potential temperatures up to 410 K at various stages of the vortex breakdown. Detailed observations of chlorine species during PGS-14 are presented in the "Highlighted results" section (Fig. 15). During the

Table 3. Overview of PGS flights of phase 2 (midwinter). Date, mission scope, target region, additional observations/ remarks, and operational flight data are given (EDMO = Oberpfaffenhofen, Germany).

Flight No.	Date	Primary mission scope	Research topics	Target region	Additional observations/ remarks	Operational flight data
PGS-06	12 Jan 2016	Transfer flight to Kiruna with detour to Malta	Cross vortex edge and polar jet at ~40°N; midwinter conditions (inside/outside vortex)	Southern Europe (Malta) to North Atlantic (35°–72°N)	Long transect from subtrop. air masses to vortex core and cold pool; filaments of DNO_y, ClO_x, $ClONO_2$	· Base: EDMO to Kiruna · Duration: 9 h 53 min · Max FL: FL 450
PGS-07	18 Jan 2016	Filamented polar stratospheric air over Scandinavia	Probe forecasted renitrification and enhanced ClO_x at vortex edge; gravity waves over southern Norway	Scandinavia from Kiruna to Denmark	Tropospheric filament with low O_3/high N_2O; enhanced HNO_3 and nitrogen containing particles detected	· Base: Kiruna · Duration: 5 h 01 min · Max FL: FL 470
PGS-08	20 Jan 2016	Polar survey flight under cold conditions ($T < T_{NAT}$)	De-/renitrification, chlorine activation, possible PSCs at flight level; tropopause fold	North Atlantic and Arctic Oceans between Scandinavia and Iceland (87°N)	Minimum T at flight level: –76°C; up to 7 ppbv of HNO_3 at FL 480, PSC particles (containing H_2O and HNO_3) at FL480	· Base: Kiruna · Duration: 9 h 53 min · Max FL: FL 480
PGS-09	22 Jan 2016	*CALIPSO* validation flight in cold air	Measure PSCs in the cold pool east of Greenland (high tropopause and $T < T_{NAT}$); fly along two (advected) *CALIPSO* overpass tracks in the North Atlantic	Arctic Ocean between northern Scandinavia and northeastern Greenland	Seven dropsondes released into polar low below aircraft for temperature comparison with GLORIA; large-scale PSCs observed by WALES	· Base: Kiruna · Duration: 8 h 15 min · Max FL: FL 480
PGS-10	25 Jan 2016	Gravity wave research over Iceland	Explore gravity waves over Iceland; fly through cirrus clouds at low flight levels (FL 370–FL 410); fly through WCB outflow region	Arctic Ocean between northern Scandinavia and Iceland with a focus on gravity waves over Iceland	Hexagon-shape profile for tomographic measurements of gravity waves with GLORIA, dropsondes for temperature comparison with GLORIA; enhanced HNO_3 and nitrogen containing articles detected	· Base: Kiruna · Duration: 7 h 46 min · Max FL: FL 470
PGS-11	28 Jan 2016	Explore mountain-wave situation in coordination with Falcon flight	Explore transient mountain-wave situation and tropopause structure by in situ and remote sensing sensors	Southern Scandinavia	Coordinated flight with Falcon for gravity wave detection at various flight levels	· Base: Kiruna · Duration: 6 h 47 min · Max FL: FL 450
PGS-12	31 Jan 2016	Late January survey and iso-SZA flight leg to test chlorine/bromine kinetics with DOAS	Cross tropopause from Arctic stratosphere into subtropical air at southernmost point over Ireland; search for enhanced NO_y and activated chlorine	North Atlantic and Arctic Oceans between Ireland and 77°N	Passing jet stream over Ireland at wind speeds up to 200 kt (~103 m s^{-1}) strongly filamented transition region	· Base: Kiruna · Duration: 9 h 06 min · Max FL: FL470
PGS-13	2 Feb 2016	Gravity wave research; high-latitude survey	Investigate gravity waves over Spitsbergen; high-latitude survey below cold pool	Arctic Ocean (67°–87°N, ~20°E)	Hexagon-shape flight profile at FL 450 for tomographic measurements with GLORIA and coordinated dropsonde releases	· Base: Kiruna · Duration: 7 h 23 min · Max FL: FL 470 · End of mission phase 2

southward leg of PGS-14 over Baffin Island, strongly subsided air masses were measured with volume mixing ratios of over 1,200 ppb for ozone [Fast and Accurate In Situ Ozone Instrument (FAIRO)], 203 ppb for N_2O (TRIHOP), and 7.05 ppt for SF_6 [Gas Chromatograph for the Observation of Stratospheric

Table 4. Overview of PGS flights of phase 3 (late winter–spring). Date, mission scope, target region, additional observations/remarks, and operational flight data are given (EDMO = Oberpfaffenhofen, Germany).

Flight No.	Date	Primary mission scope	Research topics	Target region	Additional observations/ remarks	Operational flight data
PGS-14	26 Feb 2016	Late February survey at different theta levels reaching strongly subsided air masses	PSCs; hunting of stratospheric cold pool above FL, signs of mixed-in extravortex air at FLs; probe ClO production on legs on iso-SZA legs	Scandinavia to Baffin Island crossing Greenland at different latitudes	Strongly subsided air masses between Greenland and Canada, characterized by low N_2O, high DO_3, ClO_x, DNO_y and $ClONO_2$; release of dropsondes	· Base: Kiruna · Duration: 9 h 40 min · Max FL: FL 470 · Beginning of mission phase 3
PGS-15	29 Feb 2016	Probing a polar low and gravity waves above northern Scandinavia	Explore gravity waves associated to a polar low; probe cold cirrus clouds; search for possible in situ chlorine activation	Norwegian coastal area	Staged flight levels to probe structure of polar low	· Base: Kiruna · Duration: 7 h 24 min · Max FL: FL 470
PGS-16	6 Mar 2016	Gravity wave research over Greenland combined with filament	Gravity waves; observe subsided air masses at different FLs; probe cirrus clouds at FL 360 over Kiruna on return	North Atlantic between polar circle, Iceland, and southern Greenland	Crossing of filaments southwest of Iceland at different flight levels; fuel stop in Keflavik, Iceland	· Base: Kiruna-Keflavik-Kiruna · Duration: 10 h 24 min · Max FL: FL 470
PGS-17	9 Mar 2016	Probing air masses with high theta west of Greenland	Probe a second time the aged vortex air masses (two weeks after PGS-14) with low N_2O, high total chlorine, and potentially large ozone loss	Long transect to Baffin Island, reaching 72°W; focus on area between Greenland and Baffin Island	Fuel stop at Kangerlussuaq, Greenland	· Base: Kiruna to Kangerlussuaq to Kiruna · Duration: 10 h 23 min · Max FL: FL 470
PGS-18	10 Mar 2016	Gravity wave observations over northern Greenland	Observe gravity waves; probe high-N_2O air masses on way back.	Scandinavia to northeast Greenland	Dropsondes	· Base: Kiruna · Duration: 7 h 54 min · Max FL: FL 470
PGS-19	13 Mar 2016	Transfer flight to EDMO via Kangerlussuaq (BGSF); spring survey	Observe air masses with low N_2O over northwest Greenland; probe high tropopause above North Atlantic section	Arctic Sea between Scandinavia and Greenland, North Atlantic, Germany	Long transects from Kiruna to northwestern Greenland and back to Germany via southwestern Greenland	· Base: Kiruna to Kangerlussuaq to EDMO · Duration: 10 h 19 min · Max FL: FL 470
PGS-20	16 Mar 2016	Southbound survey flight	Horizontal tropopause cut at high altitude; access a wide range of equivalent latitude and distance to the tropopause	Germany to Canary Islands via France, Spain, Atlantic Ocean west of Africa; southernmost point: 25°N	SALSA flight; fuel stop at Faro, Portugal	· Base: EDMO to Faro to EDMO · Duration: 9 h 27 min · Max FL: FL 470
PGS-21	18 Mar 2016	Match flight for air masses probed during PGS-19 and cirrus	Probe polar vortex air masses that were probed before on PGS-19 over Greenland; observe cirrus clouds at different flight levels in situ and by using the lidar	Germany, Scandinavia	Fuel stop in Kiruna to reach high flight levels	· Base: EDMO to Kiruna to EDMO · Duration: 7 h 43 min · Max FL: FL 470

Tracers (GhOST)]. During PGS-14 PSCs were still present across the North Atlantic sector.

The flight PGS-15 was devoted to study a polar low approaching the Norwegian coast associated with gravity waves, and flights PGS-16 and PGS-18 were focusing on gravity wave situations over Greenland.

The transfer flight (PGS-19) back to Oberpfaffenhofen took place on 13 March, with a detour over Greenland to probe again patterns of aged vortex air at high θ levels. Finally, two flights were performed from Oberpfaffenhofen. PGS-20 went toward the Canary Islands (25°N) to cover the transition region between middle and low latitudes in spring with respect to SALSA science objectives. PGS-21 studied once again and for the last time aged vortex air situated over northern Scandinavia when patches of enhanced $ClONO_2$ were still measured by GLORIA (Fig. 16).

HIGHLIGHTED RESULTS. The following section presents briefly selected scientific highlights achieved from the POLSTRACC mission for the Arctic winter 2015/16 for the following topics: 1) synergy between in situ and remote sensing instruments and cross validation, 2) state of polar vortex: transport and mixing, 3) case study of a tropopause fold at the polar-front jet stream with vertically propagating mountain waves, 4) large-scale ice PSCs, 5) denitrification of the stratosphere and extensive nitrification of the LMS, and 6) halogen chemistry and ozone depletion in the Arctic lowermost stratosphere.

Synergy between in situ and remote sensing instruments and cross validation. The combination of in situ and remote sensing instruments in the POLSTRACC payload enabled us to extend the findings sampled in situ at flight altitude throughout the lowermost stratosphere and sometimes even across the tropopause into the Arctic upper troposphere. Comparisons between in situ instruments and the GLORIA limb sounder are shown in Figs. 7a–f. These comparisons show an overall agreement and also reflect the different data precisions and temporal resolutions of the measurements. Differences between these datasets mostly result from atmospheric variability, as measurements of the in situ instruments are recorded directly at the aircraft, while remote sensing instruments sample air masses along the whole line of sight through the atmosphere although with a strong weight around the tangent altitude. Due to these different measurement geometries, atmospheric variabilities with horizontal gradients lead to differences in the observed trace gases between in situ and remote sensing measurements. Interestingly, particularly strong discrepancies are manifested in comparisons of HNO_3, $ClONO_2$, and O_3 at similar parts of the flight which indicates strongly filamented structures along the GLORIA line of sight (Johansson et al. 2018).

In addition, GLORIA and WALES measurements of O_3 have been compared to ozone sondes, launched from Ny-Ålesund and these comparisons are presented in Figs. 7g and 7h. GLORIA measurements during flight PGS-08 on 20 January 2016, spatially close to Ny-Ålesund show on average an agreement with the profile measured by the ozone sonde within 25 ppbv, even in the upper troposphere. This comparison extends the finding of Johansson et al. (2018), who found GLORIA O_3 retrievals to agree with FAIRO in situ O_3 measurements within the estimated errors of the instruments. Ozone measurements above the aircraft were possible with the WALES instrument during flight PGS-05 on 21 December 2015. The comparison with a coordinated ozone sonde, launched from Ny-Ålesund, shows agreement between the averaged WALES profiles, which have been recorded close to the ozone sonde.

State of polar vortex: Transport and mixing. An overview of the trace gas measurements during POLSTRACC is presented in Fig. 8 and Fig. 9 as a function of equivalent latitude and potential temperature (e.g., Hoor et al. 2004; Engel et al. 2006). Equivalent latitude is calculated from potential vorticity and thus together with potential temperature is conserved for adiabatic and reversible transport. Changes in the mean tracer distributions in potential temperature–equivalent latitude space correspond to diabatic and irreversible transport and mixing. Due to the prevailing very cold temperatures in the LMS during December 2015 and January 2016, the potential temperatures reached during POLSTRACC phase 1 at high (equivalent) latitudes were limited to about 370 K. In contrast, during March 2016 we could probe high-latitude air masses up to 410-K potential temperatures. Mean age of air is calculated from SF_6 measurements of the GhOST instrument reaching up to 5 years in late February and March in high-latitude air in the LMS. These old mean ages correspond to air masses with inorganic chlorine (Cl_y) of about 2 ppbv. Diabatic subsidence of air masses from the polar vortex into the lower and lowermost high-latitude stratosphere lead to an ageing of air, together with a decrease in N_2O. Interestingly, Krause et al. (2018) find that the polar lower stratosphere showed at the same time an increase in mean age, as well as an increase in tropospheric carbon monoxide (CO). This is strong evidence for mixing of younger (or

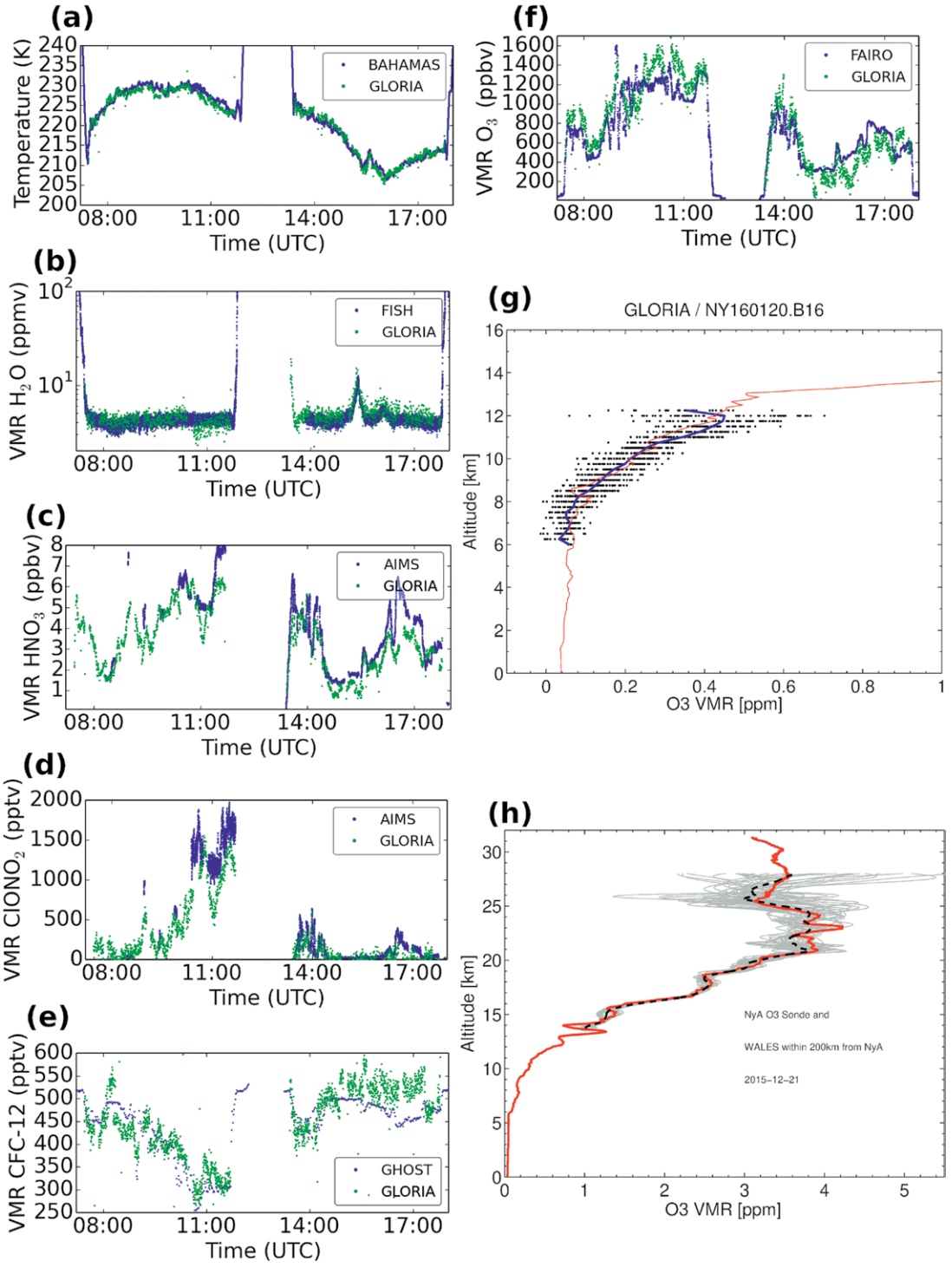

Fig. 7. (a)–(f) Comparison of the GLORIA measurements (green) to in situ measurements (blue) at flight altitude of PGS-19 on 13 Mar 2016 for (a) temperature, (b) H_2O, (c) HNO_3, (d) $ClONO_2$, (e) CFC-12, and (f) O_3. (g) Ozone profiles from GLORIA observations during flight PGS-08 on 20 Jan 2016 compared to a coincident ozone sounding at Ny-Ålesund (red solid line). Black dots show individual O_3 retrievals of GLORIA for tangent point locations within 100 km from Ny-Ålesund; thick solid line shows the average GLORIA profile. The tropopause was located at about 9-km altitude. The GLORIA and ozone sonde observations agree within 25 ppb. Excellent agreement is achieved both in the lower stratosphere and in the upper troposphere. (h) Ozone profile observations from the WALES lidar instrument during flight PGS-05 on 21 Dec 2015 with the coordinated ozone sonde at Ny-Ålesund, Spitsbergen (79°N, 11°E; red solid line). Gray lines are individual WALES profiles within 200 km from Ny-Ålesund; black dashed line represents the averaged WALES profile.

tropospheric) air masses into the polar stratosphere. Simulation with the CLaMS model reproduce this change in the age of air spectrum, with a general aging and a simultaneous increase in the fraction of young air (Krause et al. 2018). Nevertheless, N_2O observations in comparison to previous Arctic winters indicate that the 2015/16 Arctic polar vortex was rather unperturbed until early March with little in-mixing of outside vortex air.

Tropopause fold at the polar-front jet stream with vertically propagating mountain waves. On 12 January 2016, the polar-front jet stream was located above northern Italy. At the same time, mountain waves

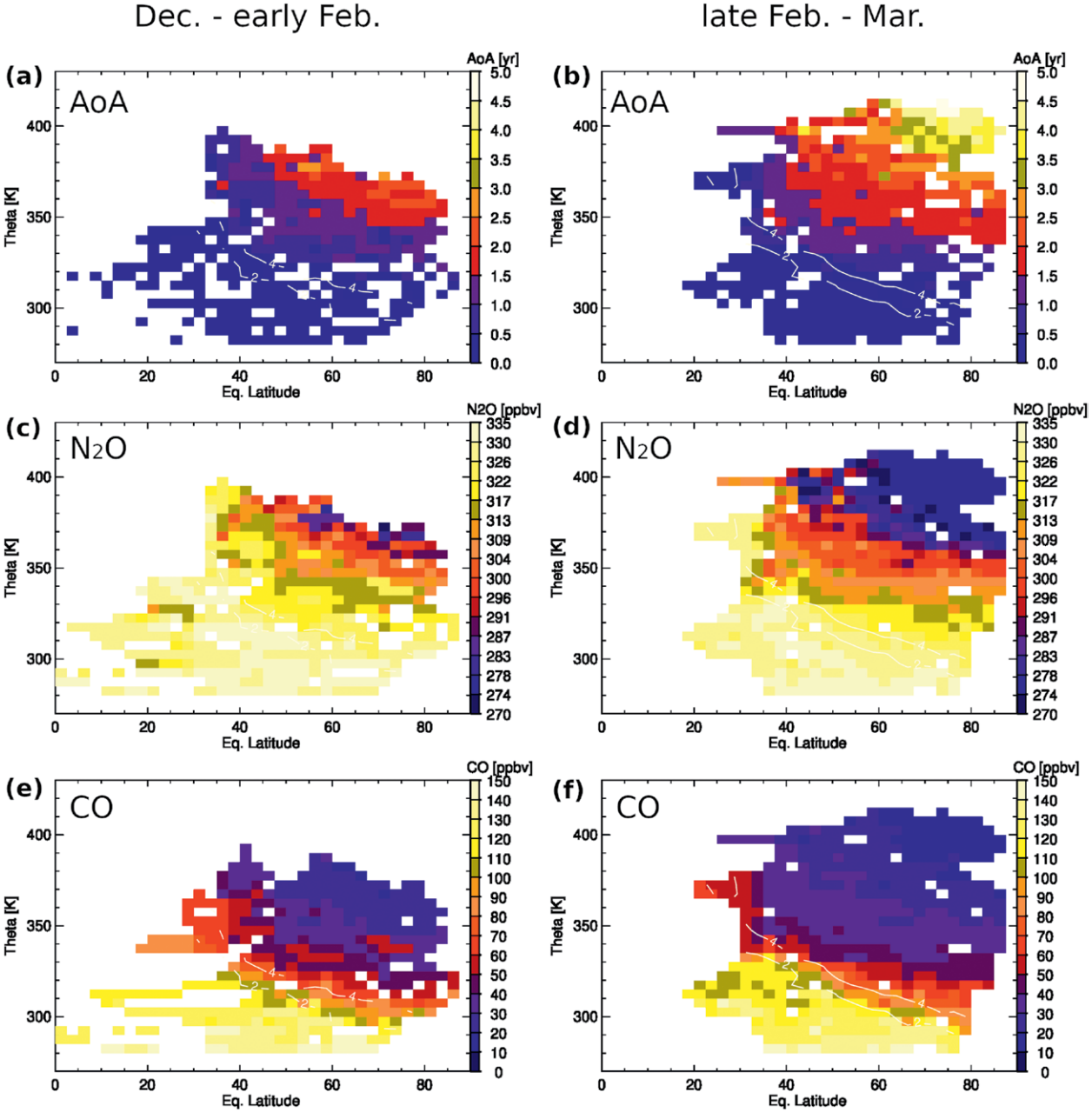

Fig. 8. Overview of trace gas observations and derived age of air during POLSTRACC as a function of equivalent latitude and potential temperature for flights during (a),(c),(e) December 2015, January and early February 2016 and (b),(d),(f) late February and March 2016. (top) Mean age of air (AoA; yr), derived from GhOST SF_6 measurements. (middle) N_2O from TRIHOP observations. (bottom) Carbon monoxide (CO) from TRIHOP observations. White contour lines indicate the 2- and 4-PVU potential vorticity levels (1 PVU = 10^{-6} K kg^{-1} m^2 s^{-1}), as an indication for the dynamical tropopause. Adapted from Krause et al. (2018).

were excited above the French Alps, Corsica–Sardinia, and the Apennines and resulted in an unexpected stall event of HALO during PGS-06, requiring intervention by the pilots (Bramberger et al. 2018). Mountain waves carried large vertical energy fluxes of 8 W m^{-2} and propagated vertically from the troposphere to the stratosphere without significant dissipation. Below the same flight section, GLORIA observations resolved the mesoscale fine structure of a tropopause fold at the polar-front jet stream in interaction with a mountain wave (Woiwode et al. 2018). The GLORIA observations show dry intrusions into the troposphere at the cyclonic shear side of the jet stream, and moist air entraining into the stratosphere at the anticyclonic shear side (Fig. 10). Tracer–tracer correlations of water vapor and ozone as a function of potential temperature constructed from the GLORIA observations resolve an active mixing region, which is perturbed by vertically propagating mountain waves. The study confirms the conceptual model of tropopause folds (Shapiro et al. 1980), validates the high quality of short-term deterministic forecasts by the ECMWF Integrated Forecast System (IFS), and

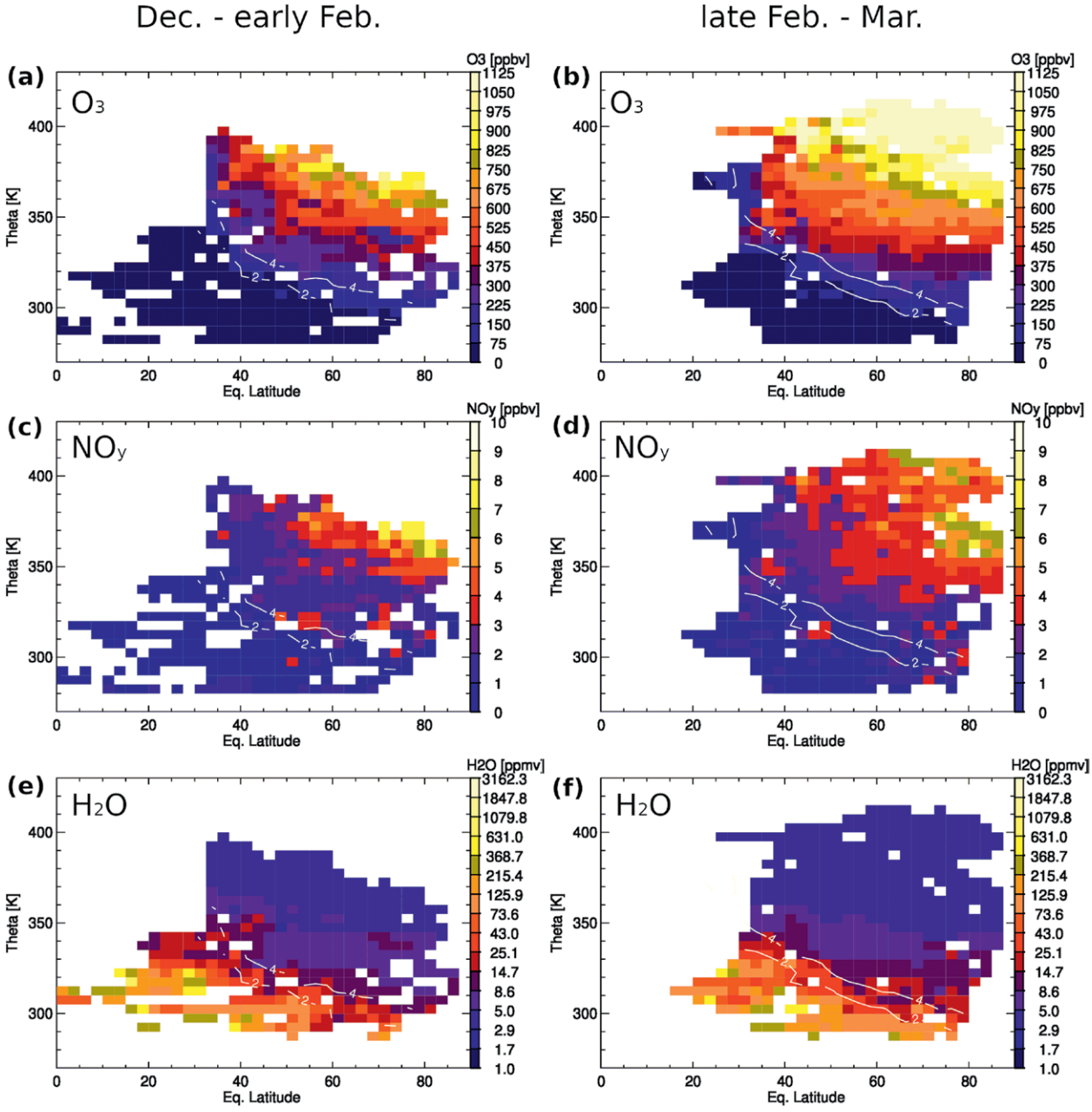

Fig. 9. As in Fig. 8, but for (top) ozone, (middle) NO_y, and (bottom) water vapor. Adapted from Krause et al. (2018).

suggests that mountain waves modulate exchange processes associated with tropopause folds.

Large-scale ice PSCs in the extremely cold 2015/16 Arctic stratospheric winter. The cold winter conditions during winter 2015/16 (Manney and Lawrence 2016; Dörnbrack et al. 2016) set the stage for excessive large-scale PSC formation. Thus, in January 2016, the CALIOP instrument on board the *CALIPSO* satellite measured the largest PSC coverage throughout its 11-yr climatology in the Arctic (Pitts et al. 2018). A three-dimensional visualization of the Arctic PSC observed on 22 January 2016, the day of PGS-09 is shown in Fig. 11. The version 2.0 CALIOP PSC detection algorithm (Pitts et al. 2018) is used to calculate total backscatter ratios at 532 nm, that is the ratio of total backscatter to molecular backscatter (Pitts et al. 2013). Single orbits are merged to the composite plot of backscatter ratios observed by *CALIPSO* on 22 January 2016. The vertical and horizontal extension of the PSC with a volume larger than 7×10^7 km^3 exceeds PSC coverage in any other year of the climatology (Pitts et al. 2018).

PSCs above HALO flight altitudes were detected with the WALES lidar instrument on board HALO (Wirth et al. 2009; Grooß et al. 2014). On 22 January 2016, a widespread PSC was measured on flight PGS-09 from Kiruna to Greenland over a horizontal distance larger than 2,200 km (Fig. 12). The phase of the PSC was derived from backscatter and depolarization information in the cloud as described in Voigt et al. (2018). High backscatter and depolarization ratios, indicative for polar stratospheric ice clouds, were detected in a cloud layer with a vertical thickness of 2–4 km over distances of several hundred kilometers. The synoptic-scale ice PSC particles

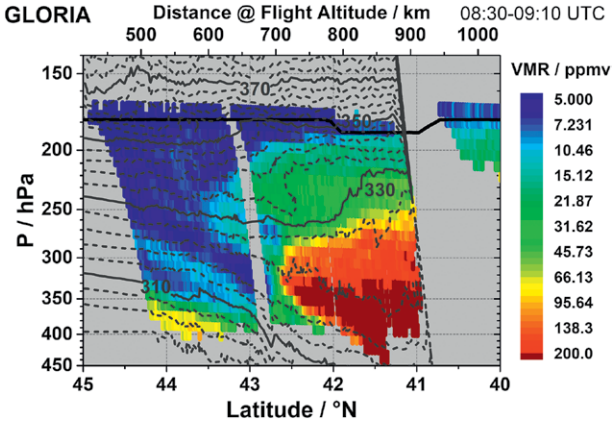

Fig. 10. GLORIA observations of water vapor (color coding) on 12 Jan 2016 (PGS-06), resolving the mesoscale fine structure of a tropopause fold at the polar-front jet stream. Isolines of potential temperature calculated from GLORIA measurements are superimposed (solid and dashed gray lines; ΔΘ = 4 K). The black solid line indicates the HALO flight altitude. Reprint from Woiwode et al. (2018), CC Attribution 4.0 License.

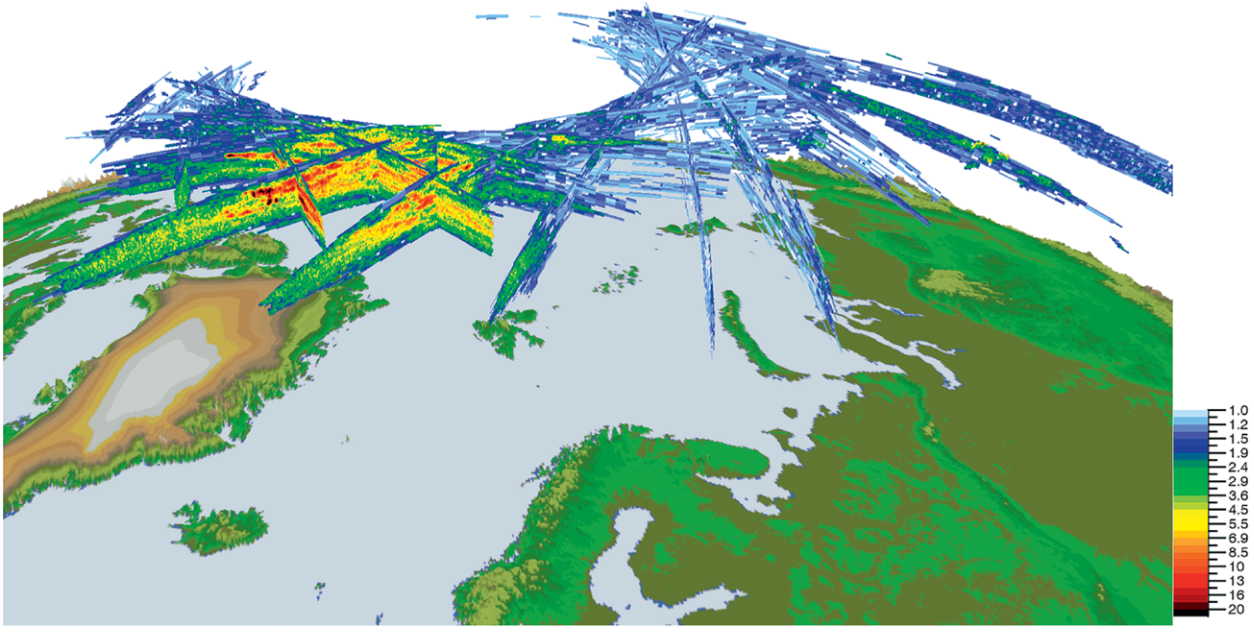

Fig. 11. Total backscatter ratio data (shaded) from the 15 *CALIPSO* orbits on 22 Jan 2016 (the day of PGS-09) in northern latitudes. Single orbits are separated in time by 99 min. Orange to red colors are indicative of ice PSCs, blue and green regions are covered by NAT, STS, or a mixture of them. The geometry is stretched in the vertical by a factor of 40.

were surrounded by cloud layers mainly consisting of NAT, nondepolarizing liquid STS droplets as well as their mixtures (Voigt et al. 2018). Large-scale Arctic ice PSCs were only observed by *CALIPSO* in the 2009/10 Arctic winter but with lower ice area coverage than in 2015/16 (Pitts et al. 2018). The ice PSC has

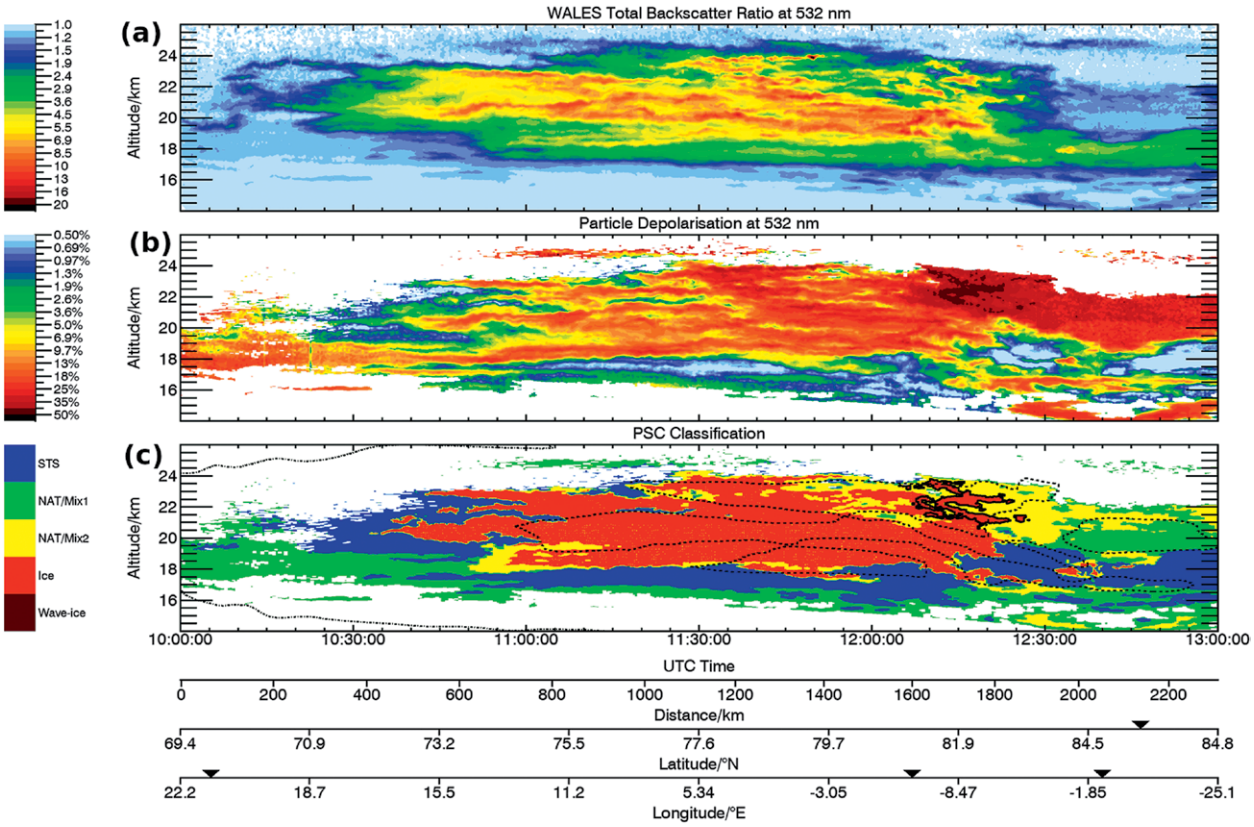

Fig. 12. (a) Lidar observation of synoptic-scale polar stratospheric ice clouds. Backscatter ratios from the WALES high-spectral-resolution lidar (Wirth et al. 2009) at 532-nm wavelength during the PGS-09 flight into the Arctic vortex on 22 Jan 2016. (b) Combined with information on particle depolarization, (c) the PSC type can be inferred as described in Voigt et al. (2018). The large-scale ice PSC in the center [(red in (c)] is embedded in mixed NAT and liquid STS cloud layers. In addition, the areas with temperatures below T_{NAT} (Hanson and Mauersberger 1988; dotted outer line) and T_{ice} (dashed line) are shown. The solid black line bounds the fraction of the ice PSC, which could have nucleated on NAT (Voigt et al. 2018). Modified from Voigt et al. (2018), CC Attribution 4.0 License.

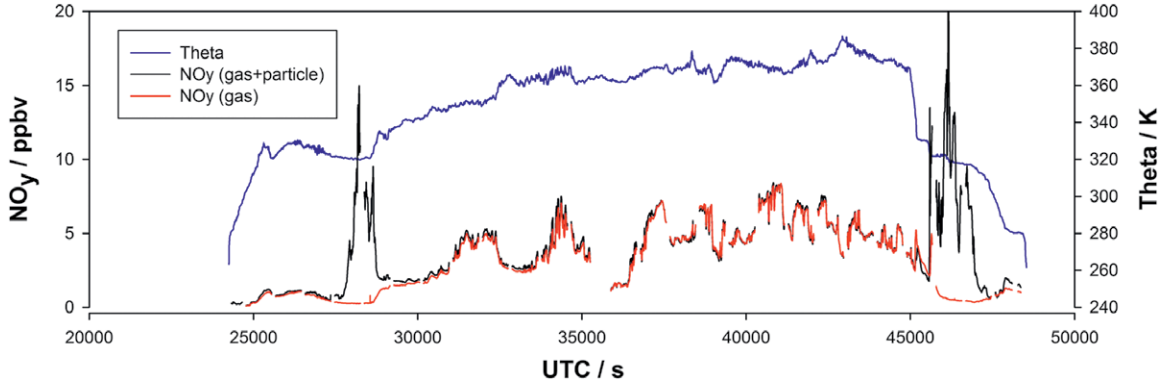

Fig. 13. Time series of measured total reactive nitrogen during the flight PGS-10 on 25 Jan 2016. Gas-phase NO_y is shown in red; total NO_y (gas phase + enhanced sampled particle NO_y) is shown in black. Potential temperature is given in blue. Total NO_y is not corrected for the enhancement.

two branches with high or low particle depolarization ratio, indicative for different ice nucleation pathways. Ice nucleation on NAT (Voigt et al. 2018) may account for the higher particle depolarization ratios while ice nucleation in STS with meteoric inclusions (Engel et al. 2013) may contribute to the lower branch. The observation of widespread Arctic ice PSCs in the winter 2015/16 advances the knowledge on ice PSC nucleation. The new observational database can be used for model evaluation in polar latitudes. In addition to dehydration, the ice PSCs can contain traces of nitric acid, which may substantially contribute to renitrification as observed in the Arctic winter 2015/16.

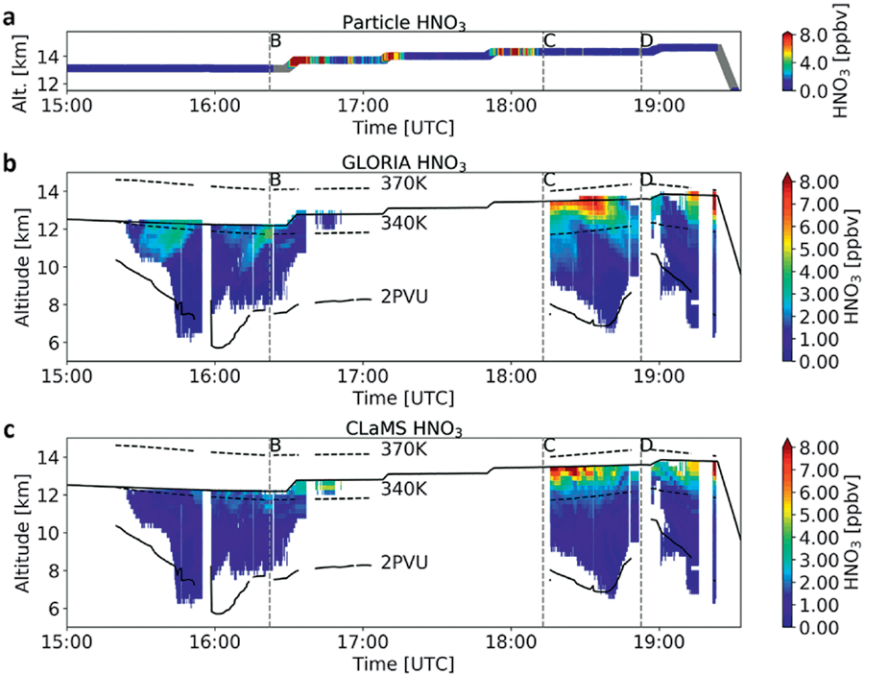

Fig. 14. Extensive and ongoing nitrification of the Arctic LMS as measured during the HALO flight on 20 Jan 2016 (PGS-08). (a) Estimated particulate NO_y at flight altitude from in situ measurements of total NO_y, without enhancement correction. (b) GLORIA vertical cross section of gas-phase HNO_3, showing local maxima in close vicinity to enhanced particulate NO_y. Note that some of the structures are partly of dynamical origin (e.g., points C to D) and are partly found also in GLORIA O_3 observations (not shown), while narrow filaments (e.g., at point B) of excess HNO_3 have no equivalent in the O_3 distribution and suggest recently nitrified air masses. (c) CLaMS simulation of gas-phase HNO_3, capturing similar structures observed by GLORIA, but differing on fine scales and extent of nitrification. Flight altitude (thick black line), defined waypoints (labeled B, C, and D), potential temperature levels within the LMS (340 and 370 K, from ECMWF; dashed black lines) and the 2-PVU level (from ECMWF; black line) as an indicator for the dynamical tropopause are indicated. Modified from Braun et al. (2019), CC Attribution 4.0 License.

Denitrification of the stratosphere and extensive nitrification of the LMS. While denitrification of the polar stratosphere by HNO_3-containing PSC particles is a well-known phenomenon (Fahey et al. 1990, 2001; Waibel et al. 1999), less attention has been paid to associated nitrification of lower layers due to sublimation of the particles. As a consequence of cold temperatures in the Arctic winter 2015/16, denitrification of layers above ~100 hPa and associated nitrification of lower layers were found in satellite-borne observations (Khosrawi et al. 2017). An exceptional finding during the POLSTRACC flights was the detection of large HNO_3-containing particles at around 14 km by the in situ instrument AENEAS. An example is shown for PGS-10 in Fig. 13. The observations show that these particles sediment down into the LMS under sufficiently cold conditions and make up a substantial proportion of total available NO_y.

Frequently, extensive nitrification of the Arctic LMS was diagnosed using two-dimensional vertical cross sections of gas-phase HNO_3 measured by GLORIA across wide ranges and down to potential temperatures well below 340 K or 12 km, respectively, as shown exemplary for PGS-08 in Fig. 14 (Braun et al. 2019). High maximum HNO_3 mixing ratios of locally up to 11 ppbv were observed, and HNO_3 enhancements due to nitrification between 5 and 7 ppbv were derived from the GLORIA measurements in January based on tracer–tracer correlations (Braun et al. 2019). Fine structures in the gas-phase HNO_3 distribution suggest recently nitrified regions. Nitrification of the LMS was also derived during the same flight from in situ observations using the well-established correlation between total reactive nitrogen (NO_y) and nitrous oxide (N_2O), yielding excess NO_y values up to 6 ppbv, in good agreement with the GLORIA observations. Comparisons of mesoscale structures in gas-phase HNO_3 observed by GLORIA with CLaMS

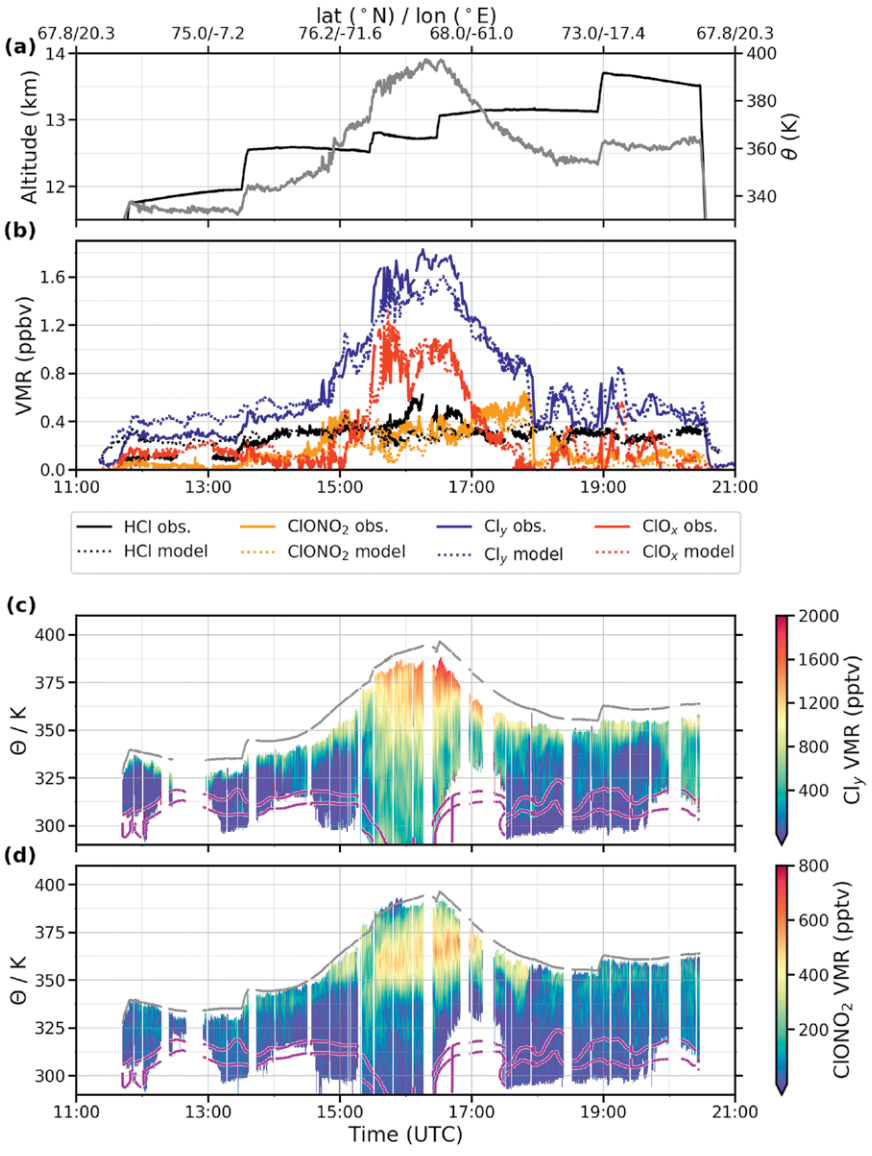

Fig. 15. Time series of measurements during flight PGS-14 on 26 Feb 2016. (a) Altitude (left axis) and potential temperature θ (right axis) and (b) chlorine species from in situ measurements. Solid lines indicate measurements and dashed lines denote CLaMS simulations interpolated along the flight track. GLORIA observations of (c) Cl_y (calculated from observed CFC-12 using the same correlation as for the GhOST data) and (d) $ClONO_2$.

simulations also agree. However, significant differences remain in the fine structures, and nitrification of the LMS is underestimated by several parts per billion by volume by the model. Sensitivity experiments using CLaMS suggest that details of the particle microphysics are needed to explain the data until the end of January, while air subsidence, transport, and mixing increasingly affect nitrification patterns in the LMS rather toward the end of the winter (Braun et al. 2019). Until mid-March 2016, air masses depleted in NO_y descended down and became accessible to the in situ instruments onboard HALO. At that time, the correlation with N_2O reveals deviations from the expected NO_y volume mixing ratio by up to ~5 ppbv at a potential temperature of ~400 K (Fig. ES11 in supplemental material).

Chlorine–bromine chemistry in the Arctic lowermost stratosphere. As noted above, the cold temperatures in the Arctic lower stratosphere in winter 2015/16 led to widespread occurrence of polar stratospheric clouds over a large altitude range, reaching down to HALO flight altitudes. The POLSTRACC observations allowed us to study in detail the halogen partitioning and ozone loss in the lower and lowermost Arctic stratosphere. The amount of available inorganic chlorine in the lowermost stratosphere is controlled by subsidence within the polar vortex and mixing across the vortex edge. Available inorganic chlorine (Cl_y) was derived from GhOST CFC-12 observations using a correlation based on whole air sampler measurements from balloon-borne observations in the Arctic stratosphere (Wetzel et al. 2015), updated for current tropospheric chlorine source gas mixing ratios. The sum of in situ measured HCl and $ClONO_2$ from AIMS agreed very well with the estimated Cl_y for many flights, but sometimes falls considerably short, indicating the presence of active chlorine compounds. An interesting case study is provided by PGS-14 on 26 February 2016. High values of Cl_y were observed, reaching 1.7 ppbv at potential temperatures of 380 K and above (Figs. 15a,b). For this situation, the sum of observed HCl and $ClONO_2$, however, is substantially

smaller than inferred Cl_y, suggesting a significant contribution from active chlorine, ClO_x (defined here as the difference between Cl_y and the sum of HCl and $ClONO_2$) of up to 1.2 ppbv (Fig. 15; see also Marsing et al. 2019). In fact, the Cl_y and ClO_x concentrations derived from the in situ observations agree very well with calculations from the CLaMS model. GLORIA observations (Johansson et al. 2018, 2019) provided simultaneous observations on the vertical extent of the chlorine processing in the lowermost stratosphere (Figs. 15c,d). Cl_y levels of about 1 ppbv and more extended down to potential temperatures of about 350 K. $ClONO_2$ was reduced at flight altitudes, consistent with a large contribution of active chlorine at potential temperatures above 380 K. Higher concentrations of $ClONO_2$ with peak mixing ratios of about 0.5 ppbv were observed lower down between 350 and 380 K.

Measurements by GLORIA of two-dimensional distributions of $ClONO_2$ over the course of the winter were used to evaluate the chlorine partitioning in the CTM CLaMS and the CCM EMAC. A comparison of flights PGS-06 (12 January 2016), PGS-14 (26 February 2016), and PGS-21 (18 March 2016) is shown in Fig. 16. These comparisons reveal that CLaMS succeeds to reproduce even small-scale structures in the trace gas distributions, while EMAC is able to reflect the overall structure of measured $ClONO_2$ enhancements. Remaining differences can be explained by the lower spatial resolution of the EMAC model. Interestingly, both models underestimated maximum mixing ratios of $ClONO_2$ for the late winter flight PGS-21, which indicates that the diabatic descent over the course of the winter is underestimated in the meteorological analyses, which define dynamics in both simulations. In addition, it was found that CLaMS tends to overestimate $ClONO_2$ at potential temperature altitudes of 325–350 K, which is suspected to result from the lower boundary condition of the model (Johansson et al. 2019).

Information on bromine comes from observed source gases, including very short-lived bromine containing source gases (VSLS) and measurements of bromine monoxide (BrO) from the mini-DOAS instrument. Figure 17 shows observed BrO and estimated Br_y from source gas observations in comparison with CLaMS model calculations. The modeled BrO/Br_y ratio was used to infer Br_y from BrO observations. The particular flight profile in the later part of PGS-12 on 31 January 2016 under quasi-constant solar zenith angles provides ideal stable conditions for the interpretation and analysis of the BrO and OClO observation and the estimates of reactive ClO_x from inferred Cl_y and measured HCl and $ClONO_2$. The measurements of OClO and BrO

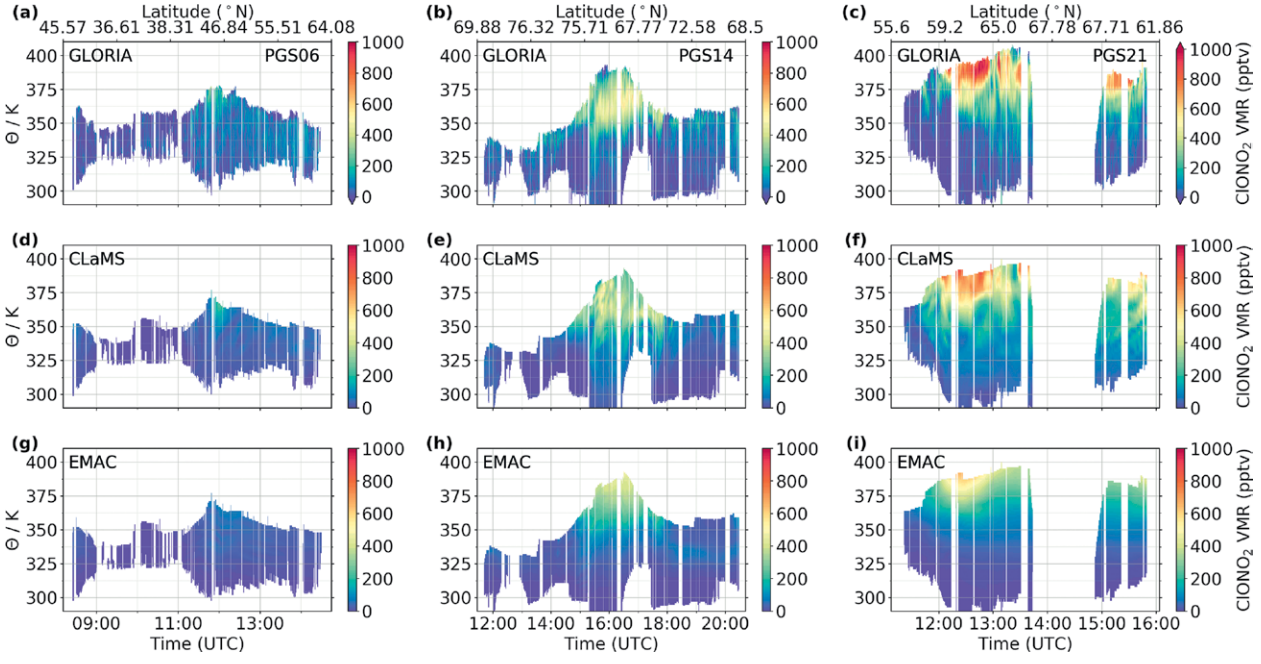

Fig. 16. Comparison of (a),(c) GLORIA-measured to (d)–(f) CLaMS and (g)–(i) EMAC-simulated $ClONO_2$ cross sections for flights (left) PGS-06 (12 Jan 2016), (center) PGS-14 (26 Feb 2016), and (right) PGS-21 (18 Mar 2016). Color bars with top and bottom arrowheads indicate data values greater and less than the color-bar range. Reprint from Johansson et al. (2019), CC Attribution 4.0 License.

support a detailed study of the efficiency of ClO_x/BrO_x ozone loss cycle for which the branching ratio of the ClO + BrO reaction into BrCl + O_2 is still somewhat uncertain (Canty et al. 2005). Further, the combined measurements of organic and inorganic bromine can be tightly monitored as a function of air mass age.

Ozone depletion in the Arctic lowermost stratosphere. Substantial ozone depletion in the lower and lowermost stratosphere, consistent with the chlorine activation in this altitude region is diagnosed from in situ and remote sensing observations of ozone during POLSTRACC. Chemical ozone depletion can be estimated by reference to a passive model tracer or through correlation with a long-lived tracer gas such as N_2O. Figure 18 shows observed ozone for 20 January and 13 March 2016, in comparison with CLaMS model simulations. The red solid line indicates the modeled passive ozone in the absence of chemical loss. On 20 January there is still little difference between the model simulations with and without photochemistry due to the limited amount of sunlight up to this time. The situation is very different in the later part of the campaign: on 13 March 2016 a large difference between the model simulations with and without chemistry emerges (red shaded area in Fig. 18, bottom), indicating chemical ozone depletion reaching more than 1 ppm or about 50% at 380 K and above by mid-March. The generally good agreement between observed and modeled ozone based on CLaMS simulations including chemistry provides confidence for the modeled passive ozone tracer as a reference to diagnose chemical ozone loss.

The agreement between the CLaMS results and observations of long-lived chemical species like ozone or N_2O indicates that the transport in the lower and lowermost stratosphere as well as the photochemistry (and microphysics) are represented well in the model. In early winter, the discrepancies between observed and modeled HCl mixing ratios are slightly larger. This is potentially caused by the same unknown processes that cause a larger discrepancy at higher altitudes in early winter (Grooß et al. 2018). The overall excellent agreement between the CLaMS model and observations of ozone and reactive chlorine and bromine species indicates that we have an adequate understanding of the processes of chlorine activation and ozone depletion in the lower and lowermost stratosphere. A realistic treatment of subsidence and mixing of air masses in this altitude range is crucial for models to properly reproduce the observed chemical ozone depletion in the Arctic

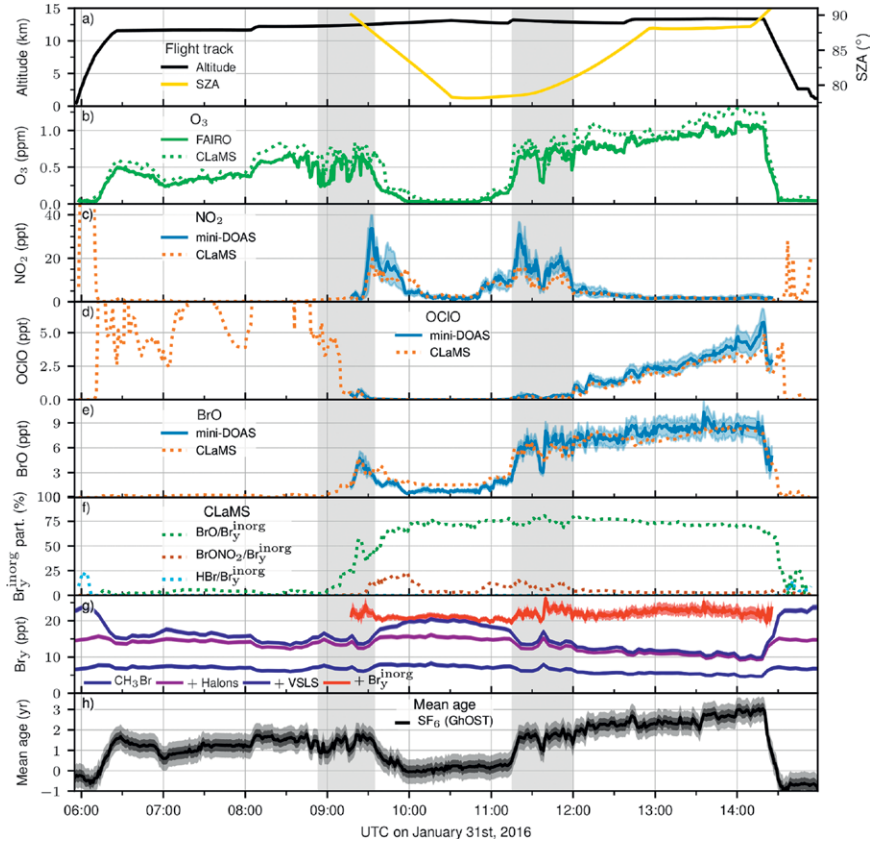

Fig. 17. Overview of flight PGS-12 on 31 Jan 2016. (a) The flight altitude and the solar zenith angle, and the gray vertical bar indicates the position of vortex edge (see text). (b) FAIRO-measured and CLaMS-modeled O_3; (c) mini-DOAS-measured and CLaMS-modeled NO_2; (d) mini-DOAS-measured and CLaMS-modeled OClO; (e) mini-DOAS-measured and CLaMS-modeled BrO; (f) CLaMS-predicted ratios for BrO/Br_y^{inorg}, $BrONO_2/Br_y^{inorg}$, and HBr/Br_y^{inorg}; (g) GHOST-measured CH_3Br (blue), to which the concentrations of the halons (purple), brominated VSLS (light blue), and inferred Br_y^{inorg} (red) are subsequently added; and (h) the mean age of air inferred from GHOST's SF_6 measurements. The shading indicates the error bar of each parameter.

UTLS region, as this controls the amount of available inorganic chlorine.

CONCLUSIONS AND OUTLOOK. The POLSTRACC Arctic aircraft campaign took place in winter 2015/16, several years after previous intensive Arctic campaigns under declining levels of ozone depleting substances (WMO 2018) and accelerated Arctic climate change (Overland et al. 2019). POLSTRACC focused particularly on the Arctic lowermost stratosphere and upper troposphere and its coupling with midlatitudes. With mission phases in December 2015, throughout January, and from late February until mid-March 2016, the campaign covered the important development of chemical and transport processes from early winter until the breakdown of the polar vortex by mid-March during the 2016 major stratospheric warming. The capabilities of the HALO research aircraft with its long-range flights and high ceiling altitude were critical for the success of the mission. From the base in Kiruna, Sweden, flights deep into the Arctic almost to the North Pole (maximum latitude reached 87.1°N during flight PGS-13) and probing high altitude air masses up to potential temperatures of 410 K were possible. Refueling stops not only allowed to extend the range, but also enabled observations at maximum flight levels in the region of interest.

The POLSTRACC payload combined precise in situ instrumentation with remote sensing instruments for measurements of temperature, trace gases, and cloud properties in the UTLS region. High-resolution ECMWF forecasts, together with chemistry transport modeling from the CLaMS model and the Mission Support System (MSS) flight planning tool (Rautenhaus et al. 2012) and satellite data from MLS and *CALIPSO*, were of great value in flight planning. The excellent agreement between the GLORIA infrared remote sensing data with in situ observations (Johansson et al. 2018) enabled us to extend the findings sampled in situ at flight altitude throughout the lowermost stratosphere and sometimes even across the tropopause into the Arctic upper troposphere. An impressive demonstration of these capabilities has been provided for a case study of a tropopause folding event and assessment of the quality of ECMWF meteorological forecasts (Woiwode et al. 2018).

The Arctic winter 2015/16 was characterized by record cold temperatures in the lower stratosphere in early winter, followed by a major warming beginning in early March. Probably one of the largest surprises during the POLSTRACC campaign was

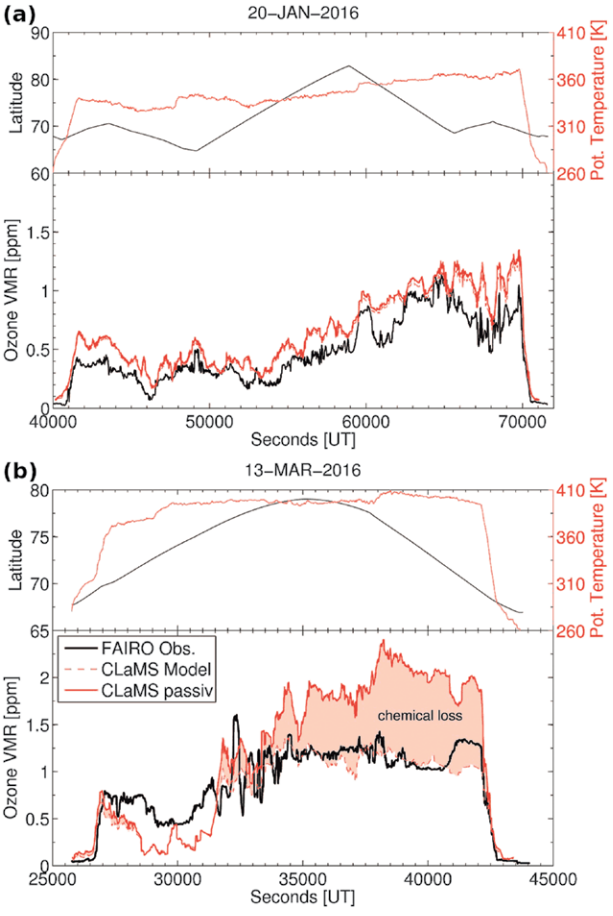

Fig. 18. Chemical ozone depletion is estimated by comparison of measured ozone to a passive ozone tracer from the CLaMS model. (a) (bottom) In situ ozone observations from the FAIRO instrument (black) for the flight on 20 Jan 2016 (PGS-08) together with simulations from the CLaMS model (red). Because there is little chemical ozone loss at this time in midwinter, passive ozone from CLaMS (red dashed line) is still similar to the fully modeled ozone. (top) Latitude (black; left axis) and potential temperature (red; right axis) are indicated. (b) As in (a), but for the flight on 13 Mar 2016 (PGS-19). Passive ozone in the absence of chemistry is now much larger than observed ozone, in particular for the second half of the flight, indicating chemical ozone depletion (red shaded area) reaching more than 1 ppm or about 50% at potential temperatures above 380 K.

the occurrence of extensive PSCs, even down to HALO flight altitude, accompanied by observation of nitrogen redistribution, chlorine activation and ongoing ozone depletion at flight altitudes. The PSC observations provided new evidence for ice nucleation on nitric acid trihydrate (NAT) particles (Voigt et al. 2018). The coordinated flight with orbits of the *CALIPSO* satellite provided an unprecedented opportunity to validate the spaceborne CALIOP lidar with independent high spectral resolution observations

by the airborne WALES lidar for an improved PSC classification. Nitric acid containing particles were observed at flight altitude—however, a quantification of the particle sizes and the amount of HNO_3 contained is challenging because of uncertainties due to the enrichments in the inlets (Afchine et al. 2018). Extensive denitrification in the lower stratosphere and a nitrification at lower altitudes were observed throughout the winter (Khosrawi et al. 2017; Braun et al. 2019). Heterogenous chlorine activation with a shift in the partitioning of inorganic chlorine from HCl toward chlorine nitrate ($ClONO_2$) was observed at different stages throughout the winter (Johansson et al. 2019), not observed in detail before at these altitudes in the Arctic. The flight under constant solar zenith angle conditions on 31 January 2016 provided a unique opportunity to study the chemistry of the BrO/OClO system and thus the ozone loss from the interhalogen reaction of ClO with BrO in the lower stratosphere from DOAS UV–visible observations.

Observations of different trace gases give a detailed picture of the impact of transport and mixing on the composition of the Arctic lowermost stratosphere throughout the winter. Subsidence of air masses from the polar vortex throughout the winter led to observed air masses with mean age of air of up to 5 years and inorganic chlorine levels of up to 2 ppm at potential temperatures between 380 and 410 K. Simultaneously with the aging of the air in the Arctic winter lower stratosphere throughout the winter, an increase in the contribution of tropospheric carbon monoxide (CO) was observed between January and March at levels up to 370 K, showing the importance of in-mixing of younger air masses into the Arctic lower stratosphere (Krause et al. 2018). The investigation of the importance of this in-mixing for the distribution of water in the lowermost stratosphere and the resulting radiative effects is currently under way, based on the POLSTRACC in situ and remote sensing observations. Substantial chemical ozone depletion was observed in the Arctic lower and lowermost stratosphere between January and late February and early March 2016, reaching local losses of up to 50%. Further studies should investigate the consequences of these large observed ozone losses in the lowermost Arctic stratosphere for radiative and dynamical coupling with the surface and troposphere and how well this is represented in current chemistry climate models. Comparison with satellite data will help to put the airborne observations in winter 2015/16 into a longer-term perspective. The winter of 2015/16 with record low temperatures in early and midwinter in the lower stratosphere was another winter in a row of record cold winters about every 5 years observed since the early 1990s (e.g., Rex et al. 2004; Sinnhuber et al. 2011; Bohlinger et al. 2014). Whether or not this is a manifestation of climate change in the Arctic stratosphere remains unclear at present as well as possible consequences of a changing Arctic. The POLSTRACC data will help to test and ultimately improve relevant chemical and transport processes in chemistry climate models.

POLSTRACC data are available through the HALO database at https://halo-db.pa.op.dlr.de/.

ACKNOWLEDGMENTS. We thank the pilots, engineers, and scientists from DLR Flight Department–Flight Experiments for their excellent support during the POLSTRACC campaign. Andreas Minikin provided vigilant overall project management and Frank Probst responsively supported the operational activities. Andreas Giez, Volker Dreiling, and Martin Zöger supervised the BAHAMAS observations. We acknowledge the cooperative spirit of the airport manager Kurt Mäki and the team of the tower of the Kiruna Airport. We thank Andreas Dörnbrack, Sonja Gisinger, Martina Bramberger, Maxi Böttcher, and Johannes Wagner for the excellent meteorological support and Reinhold Spang for support with CLaMS forecasts. Reimar Bauer contributed to extending and adapting the MSS tools to the POLSTRACC needs. Ole Kirner and Farah Khosrawi provided near-real-time EMAC simulations; Jennifer Schröter provided the ICON-ART simulations. We acknowledge the use of meteorological forecasts from the European Centre for Medium-Range Weather Forecasts (ECMWF) and the MLS satellite data. We thank Peter von der Gathen and his team for coordinated ozone sonde launches. We thank the instrument and data analysis teams of AENEAS (Michael Lichtenstern, Paul Stock, Greta Stratmann), FISH (Armin Afchine), GhOST (Ronja Heinemann, Timo Keber), GLORIA (Marleen Braun, Andreas Ebersoldt, Thomas Gulde, Michael Höpfner, Anne Kleinert, Thomas Latzko, Guido Maucher, Hans Nordmeyer, and Christof Piesch at KIT and Tom Neubert, Georg Schardt, Heinz Rongen, Markus Dick, Axel Schönfeld, and Isabell Krisch at FZJ), HAGAR (Valentin Lauther, Emil Gerhardt, Johannes Wintel), mini-DOAS (Tilman Hüneke, Oliver-Alex Aderhold, Bodo Werner), and WALES (Axel Amediek, Silke Gross, Mathieu Quatrevalet, Patrick Vranken) for persistent commitment. We gratefully acknowledge the funding by the Deutsche Forschungsgemeinschaft (DFG, German Research Foundation) within the Priority Program "Atmospheric and Earth System Research with the High Altitude and Long Range Research Aircraft (HALO)" SPP 1294 through the following grants: Andreas Engel and Peter Hoor (EN 367/13-1, HO 4225/7-1); Andreas Marsing,

Christiane Voigt, and Tina Jurkat-Witschas (VO1504/4-1 and JU3095-1/1); Klaus Pfeilsticker (PF-384/7-1, PF-384/7-2, PF384/9-1, PF384/9-2, and PF-384/16-1); C. Michael Volk (VO 1530/4-1); and Wolfgang Woiwode (WO 2160/1-1). The authors gratefully acknowledge the computing time for the CLaMS simulations granted on the JURECA supercomputer at Jülich Supercomputing Centre (JSC) under the VSR project ID JICG11 and for the EMAC and ICON-ART model simulations at the Steinbuch Center for Computing (SCC). The authors acknowledge support by the state of Baden-Württemberg through bwHPC.

REFERENCES

Afchine, A., and Coauthors, 2018: Ice particle sampling from aircraft – Influence of the probing position on the ice water content. *Atmos. Meas. Tech.*, **11**, 4015–4031, https://doi.org/10.5194/amt-11-4015-2018.

Bekki, S., and Coauthors, 2013: Climate impact of stratospheric ozone recovery. *Geophys. Res. Lett.*, **40**, 2796–2800, https://doi.org/10.1002/grl.50358.

Bernath, P. F., and Coauthors, 2005: Atmospheric Chemistry Experiment (ACE): Mission overview. *Geophys. Res. Lett.*, **32**, L15S01, https://doi.org/10.1029/2005GL022386.

Bönisch, H., A. Engel, T. Birner, P. Hoor, D. W. Tarasick, and E. A. Ray, 2011: On the structural changes in the Brewer-Dobson circulation after 2000. *Atmos. Chem. Phys.*, **11**, 3937–3948, https://doi.org/10.5194/acp-11-3937-2011.

Bohlinger, P., B.-M. Sinnhuber, R. Ruhnke, and O. Kirner, 2014: Radiative and dynamical contributions to past and future Arctic stratospheric temperature trends. *Atmos. Chem. Phys.*, **14**, 1679–1688, https://doi.org/10.5194/acp-14-1679-2014.

Bramberger, M., A. Dörnbrack, H. Wilms, S. Gemsa, K. Raynor, and R. D. Sharman, 2018: Vertically propagating mountain waves—A hazard for high-flying aircraft? *J. Appl. Meteor. Climatol.*, **57**, 1957–1975, https://doi.org/10.1175/JAMC-D-17-0340.1.

Braun, M., and Coauthors, 2019: Nitrification of the lowermost stratosphere during the exceptionally cold Arctic winter 2015/16. *Atmos. Chem. Phys.,* **19**, 13 681–13 699, https://doi.org/10.5194/acp-19-13681-2019.

Buchholz, B., A. Afchine, A. Klein, C. Schiller, M. Krämer, and V. Ebert, 2017: HAI, a new airborne, absolute, twin dual-channel, multi-phase TDLAS-hygrometer: Background, design, setup, and first flight data. *Atmos. Meas. Tech.*, **10**, 35–57, https://doi.org/10.5194/amt-10-35-2017.

Calvo, N., L. M. Polvani, and S. Solomon, 2015: On the surface impact of Arctic stratospheric ozone extremes. *Environ. Res. Lett.*, **10**, 094003, https://doi.org/10.1088/1748-9326/10/9/094003.

Canty, T., and Coauthors, 2005: Nighttime OClO in the winter arctic vortex. *J. Geophys. Res.*, **110**, D01301, https://doi.org/10.1029/2004JD005035.

Carslaw, K. S., T. Peter, and S. L. Clegg, 1997: Modeling he composition of liquid stratospheric aerosol. *Rev. Geosci.*, **35**, 125–154, https://doi.org/10.1029/97RG00078.

Dee, D. P., and Coauthors, 2011: The ERA-Interim reanalysis: Configuration and performance of the data assimilation system. *Quart. J. Roy. Meteor. Soc.*, **137**, 553–597, https://doi.org/10.1002/qj.828.

Dörnbrack, A., S. Gisinger, M. C. Pitts, L. R. Poole, and M. Maturilli, 2016: Multilevel cloud structures over Svalbard. *Mon. Wea. R*ev., **145**, 1149–1159, https://doi.org/10.1175/MWR-D-16-0214.1.

——, and Coauthors, 2018: Gravity waves excited during a minor sudden stratospheric warming. *Atmos. Chem. Phys.*, **18**, 12 915–12 931, https://doi.org/10.5194/acp-18-12915-2018.

Drdla, K., and R. Müller, 2012: Temperature thresholds for chlorine activation and ozone loss in the polar stratosphere. *Ann. Geophys.*, **30**, 1055–1073, https://doi.org/10.5194/angeo-30-1055-2012.

Engel, A., and Coauthors, 2006: Highly resolved observations of trace gases in the lowermost stratosphere and upper troposphere from the Spurt project: An overview. *Atmos. Chem. Phys.*, **6**, 283–301, https://doi.org/10.5194/acp-6-283-2006.

Engel, I., B. P. Luo, M. C. Pitts, L. R. Poole, C. R. Hoyle, J.-U. Grooß, A. Dörnbrack, and T. Peter, 2013: Heterogeneous formation of polar stratospheric clouds – Part 2: Nucleation of ice on synoptic scales. *Atmos. Chem. Phys.*, **13**, 10 769–10 785, https://doi.org/10.5194/acp-13-10769-2013.

Fahey, D. W., K. K. Kelly, S. R. Kawa, A. F. Tuck, M. Loewenstein, K. R. Chan, and L. E. Heidt, 1990: Observations of denitrification and dehydration in the winter polar stratospheres. *Nature*, **344**, 321–324, https://doi.org/10.1038/344321a0.

——, and Coauthors, 2001: The detection of large HNO3-containing particles in the winter Arctic stratosphere. *Science*, **291**, 1026–1031, https://doi.org/10.1126/science.1057265.

Farman, J. C., B. G. Gardiner, and J. D. Shanklin, 1985: Large losses of total ozone in Antarctica reveal ClO_x/NO_x interaction. *Nature*, **315**, 207–210, https://doi.org/10.1038/315207a0.

Fernandez, R., and Coauthors, 2017: Impact of biogenic very short-lived bromine on the Antarctic ozone hole during the 21st century. *Atmos. Chem. Phys.*, **17**, 1673–1688, https://doi.org/10.5194/acp-17-1673-2017.

Fix, A., F. Steinebach, M. Wirth, A. Schäfler, and G. Ehret, 2019: Development and application of an airborne differential absorption lidar for the simultaneous measurement of ozone and water vapor profiles in the tropopause region. *Appl. Opt.*, **58**, 5892–5900, https://doi.org/10.1364/AO.58.005892.

Friedl-Vallon, F., and Coauthors, 2014: Instrument concept of the imaging Fourier transform spectrometer GLORIA. *Atmos. Meas. Tech.*, **7**, 3565–3577, https://doi.org/10.5194/amt-7-3565-2014.

Goessling, H. F., and S. Bathiany, 2016: Why CO_2 cools the middle atmosphere – A consolidating model perspective. *Earth Syst. Dyn.*, **7**, 697–715, https://doi.org/10.5194/esd-7-697-2016.

Grooß, J.-U., and Coauthors, 2014: Nitric acid trihydrate nucleation and denitrification in the Arctic stratosphere. *Atmos. Chem. Phys.*, **14**, 1055–1073, https://doi.org/10.5194/acp-14-1055-2014.

——, and Coauthors, 2018: On the discrepancy of HCl processing in the core of the wintertime polar vortices. *Atmos. Chem. Phys.*, **18**, 8647–8666, https://doi.org/10.5194/acp-18-8647-2018.

Hanson, D., and K. Mauersberger, 1988: Laboratory studies of the nitric acid trihydrate: implications for the south polar stratosphere. *Geophys. Res. Lett.*, **15**, 855–858, https://doi.org/10.1029/GL015i008p00855.

Hegglin, M. I., and Coauthors, 2013: SPARC Data Initiative: Comparison of water vapor climatologies from international satellite limb sounders. *J. Geophys. Res. Atmos*, **118**, 11 824–11 846, https://doi.org/10.1002/jgrd.50752.

Hoor, P., C. Gurk, D. Brunner, M. I. Hegglin, H. Wernli, and H. Fischer, 2004: Seasonality and extent of extratropical TST derived from in-situ CO measurements during SPURT. *Atmos. Chem. Phys.*, **4**, 1427–1442, https://doi.org/10.5194/acp-4-1427-2004.

Hossaini, R., and Coauthors, 2015: Efficiency of short-lived halogens at influencing climate through depletion of stratospheric ozone. *Nat. Geosci.*, **8**, 186–190, https://doi.org/10.1038/ngeo2363.

Hüneke, T., and Coauthors, 2017: The novel HALO mini-DOAS instrument: Inferring trace gas concentrations from airborne UV/visible limb spectroscopy under all skies using the scaling method. *Atmos. Meas. Tech.*, **10**, 4209–4234, https://doi.org/10.5194/amt-10-4209-2017.

IPCC, 2013: *Climate Change 2013: The Physical Science Basis*. Cambridge University Press, 1535 pp., https://doi.org/10.1017/CBO9781107415324.

Ivy, D. J., and Coauthors, 2017: Observed connections of Arctic stratospheric ozone extremes to Northern Hemisphere surface climate. *Environ. Res. Lett.*, **12**, 024004, https://doi.org/10.1088/1748-9326/aa57a4.

Jöckel, P., and Coauthors, 2010: Development cycle 2 of the Modular Earth Submodel System (MESSy2). *Geosci. Model Dev.*, **3**, 717–752, https://doi.org/10.5194/gmd-3-717-2010.

Johansson, S., and Coauthors, 2018: Airborne limb-imaging measurements of temperature, HNO_3, O_3, $ClONO_2$, H2O and CFC-12 during the Arctic winter 2015/2016: Characterization, in-situ validation and comparison to Aura/MLS. *Atmos. Meas. Tech.*, **11**, 4737–4756, https://doi.org/10.5194/amt-11-4737-2018.

——, and Coauthors, 2019: Unusual chlorine partitioning in the 2015/16 Arctic winter lowermost stratosphere: Observations and simulations. *Atmos. Chem. Phys.*, **19**, 8311–8338, https://doi.org/10.5194/acp-19-8311-2019.

Jurkat, T., S. Kaufmann, C. Voigt, D. Schäuble, P. Jeßberger, and H. Ziereis, 2016: The airborne mass spectrometer AIMS – Part 2: Measurements of trace gases with stratospheric or tropospheric origin in the UTLS. *Atmos. Meas. Tech.*, **9**, 1907–1923, https://doi.org/10.5194/amt-9-1907-2016.

——, and Coauthors, 2017: Depletion of ozone and reservoir species of chlorine and nitrogen oxide in the lower Antarctic polar vortex measured from aircraft. *Geophys. Res. Lett.*, **44**, 6440–6449, https://doi.org/10.1002/2017GL073270.

Kaufmann, S., C. Voigt, P. Jeßberger, T. Jurkat, H. Schlager, A. Schwarzenboeck, M. Klingebiel, and T. Thornberry, 2014: In-situ measurements of ice saturation in young contrails. *Geophys. Res. Lett.*, **41**, 702–709, https://doi.org/10.1002/2013GL058276.

——, and Coauthors, 2016: The airborne mass spectrometer AIMS – Part 1: AIMS-H2O for UTLS water vapor measurements. *Atmos. Meas. Tech.*, **9**, 939–953, https://doi.org/10.5194/amt-9-939-2016.

——, and Coauthors, 2018: Intercomparison of mid-latitude tropospheric and lower stratospheric water vapor measurements and comparison to ECMWF humidity data. *Atmos. Chem. Phys.*, **18**, 16 729–16 745,https://doi.org/10.5194/acp-18-16729-2018.

Khosrawi, F., and Coauthors, 2017: Denitrification, dehydration and ozone loss during the 2015/2016 Arctic winter. *Atmos. Chem. Phys.*, **17**, 12 893–12 910, https://doi.org/10.5194/acp-17-12893-2017.

Kidston, J., A. A. Scaife, S. C. Hardiman, D. M. Mitchell, N. Butchart, M. P. Baldwin, and L. J. Gray, 2015: Stratospheric influence on tropospheric jet streams, storm tracks and surface weather. *Nat. Geosci.*, **8**, 433–440, https://doi.org/10.1038/ngeo2424.

Kirner, O., R. Müller, R. Ruhnke, and H. Fischer, 2015: Contribution of liquid, NAT and ice particles to chlorine activation and ozone depletion in Antarctic

winter and spring. *Atmos. Chem. Phys.*, **15**, 2019–2030, https://doi.org/10.5194/acp-15-2019-2015.

Konopka, P., and Coauthors, 2004: Mixing and ozone loss in the 1999–2000 Arctic vortex: Simulations with the 3-dimensional Chemical Lagrangian Model of the Stratosphere (CLaMS). *J. Geophys. Res.*, **109**, D02315, https://doi.org/10.1029/2003JD003792.

Krause, J., and Coauthors, 2018: Mixing and ageing in the polar lower stratosphere in winter 2015/2016. *Atmos. Chem. Phys.*, **18**, 6057–6073, https://doi.org/10.5194/acp-2017-955.

Krautstrunk, M., and A. Giez, 2012: The transition from FALCON to HALO era airborne atmospheric research. *Atmospheric Physics*, U. Schumann, Ed., Springer, 609–624, https://doi.org/10.1007/978-3-642-30183-4_37.

Krisch, I., and Coauthors, 2017: First tomographic observations of gravity waves by the infrared limb imager GLORIA. *Atmos. Chem. Phys.*, **17**, 14 937–14 953, https://doi.org/10.5194/acp-17-14937-2017.

Kunkel, D., and Coauthors, 2019: Evidence of small-scale quasi-isentropic mixing in ridges of extratropical baroclinic waves. *Atmos. Chem. Phys.*, **19**, 12 607–12 630, https://doi.org/10.5194/acp-19-12607-2019.

Manney, G. L., and Z. D. Lawrence, 2016: The major stratospheric final warming in 2016: Dispersal of vortex air and termination of Arctic chemical ozone loss. *Atmos. Chem. Phys.*, **16**, 15 371–15 396, https://doi.org/10.5194/acp-16-15371-2016.

——, and Coauthors, 2011: Unprecedented Arctic ozone loss. *Nature*, **478**, 469–475, https://doi.org/10.1038/nature10556.

Marsing, A., and Coauthors, 2019: Chlorine partitioning in the lowermost Arctic vortex during the cold winter 2015/2016. *Atmos. Chem. Phys.*, **19**, 10 757–10 772, https://doi.org/10.5194/acp-19-10757-2019.

Matthias, V., A. Dörnbrack, and G. Stober, 2016: The extraordinarily strong and cold polar vortex in the early northern winter 2015/2016. *Geophys. Res. Lett.*, **43**, 12 287–12 294, https://doi.org/10.1002/2016GL071676.

McKenna, D. S., P. Konopka, J.-U. Grooß, G. Günther, R. Müller, R. Spang, D. Offermann, and Y. Orsolini, 2002: A new Chemical Lagrangian Model of the Stratosphere (CLaMS): 1. Formulation of advection and mixing. *J. Geophys. Res.*, **107**, 4309, https://doi.org/10.1029/2000JD000114.

Meyer, J., and Coauthors, 2015: Two decades of water vapor measurements with the FISH fluorescence hygrometer: A review. *Atmos. Chem. Phys.*, **15**, 8521–8538, https://doi.org/10.5194/acp-15-8521-2015.

Müller, S., and Coauthors, 2016: Impact of the Asian monsoon on the extratropical lower stratosphere: Trace gas observations during TACTS over Europe 2012. *Atmos. Chem. Phys.*, **16**, 10 573–10 589, https://doi.org/10.5194/acp-16-10573-2016.

Murphy, D. M., and T. Koop, 2005: Review of the vapour pressures of ice and supercooled water for atmospheric applications. *Quart. J. Roy. Meteor. Soc.*, **131**, 1539–1565, https://doi.org/10.1256/qj.04.94.

Newman, P. A., and Coauthors, 2002: An overview of the SOLVE/THESEO 2000 campaign. *J. Geophys. Res.*, **107**, 8259, https://doi.org/10.1029/2001JD001303.

Overland, J. E., M. Wang, and J. E. Box, 2019: An integrated index of recent pan-Arctic climate change. *Environ. Res. Lett.*, **14**, 035006, https://doi.org/10.1088/1748-9326/aaf665.

Pitts, M. C., L. R. Poole, A. Lambert, and L. W. Thomason, 2013: An assessment of CALIOP polar stratospheric cloud composition classification. *Atmos. Chem. Phys.*, **13**, 2975–2988, https://doi.org/10.5194/acp-13-2975-2013.

——, L. R. Poole, and R. Gonzalez, 2018: Polar stratospheric cloud climatology based on CALIPSO spaceborne lidar measurements from 2006 to 2017. *Atmos. Chem. Phys.*, **18**, 10 881–10 913, https://doi.org/10.5194/acp-18-10881-2018.

Platt, U., and J. Stutz, 2008: *Differential Optical Absorption Spectroscopy: Principle and Applications*. Springer, 597 pp.

Rautenhaus, M., G. Bauer, and A. Dörnbrack, 2012: A web service based tool to plan atmospheric research flights. *Geosci. Model Dev.*, **5**, 55–71, https://doi.org/10.5194/gmd-5-55-2012.

Rex, M., R. J. Salawitch, P. von der Gathen, N. R. P. Harris, M. P. Chipperfield, and B. Naujokat, 2004: Arctic ozone loss and climate change. *Geophys. Res. Lett.*, **31**, L04116, https://doi.org/10.1029/2003GL018844.

Rieder, H. E., and L. M. Polvani, 2013: Are recent Arctic ozone losses caused by increasing greenhouse gases? *Geophys. Res. Lett.*, **40**, 4437–4441, https://doi.org/10.1002/grl.50835.

Riese, M. F., and Coauthors, 2012: Impact of uncertainties in atmospheric mixing on simulated UTLS composition and related radiative effects. *J. Geophys. Res.*, **117**, D16305, https://doi.org/10.1029/2012JD017751.

——, and Coauthors, 2014: Gimballed Limb Observer for Radiance Imaging of the Atmosphere (GLORIA) scientific objectives. *Atmos. Meas. Tech.*, **7**, 1915–1928, https://doi.org/10.5194/amt-7-1915-2014.

Sala, S., H. Bönisch, T. Keber, D. E. Oram, G. Mills, and A. Engel, 2014: Deriving an atmospheric budget of total organic bromine using airborne in-situ measurements from the western Pacific area during SHIVA. *Atmos. Chem. Phys.*, **14**, 6903–6923, https://doi.org/10.5194/acp-14-6903-2014.

Santee, M. L., G. L. Manney, N. J. Livesey, L. Froidevaux, M. J. Schwartz, and W. G. Read, 2011: Trace gas evolution in the lowermost stratosphere from Aura Microwave Limb Sounder measurements. *J. Geophys. Res.*, **116**, D18306, https://doi.org/10.1029/2011JD015590.

Schreiner, J., C. Voigt, A. Kohlmann, F. Arnold, K. Mauersberger, and N. Larsen, 1999: Chemical analysis of polar stratospheric cloud particles. *Science*, **283**, 968–970, https://doi.org/10.1126/science.283.5404.968.

Schröter, J., and Coauthors, 2018: ICON-ART 2.1: A flexible tracer framework and its application for composition studies in numerical weather forecasting and climate simulations. *Geosci. Model Dev.*, **11**, 4043–4068, https://doi.org/10.5194/gmd-11-4043-2018.

Shapiro, M. A., E. R. Reiter, R. D. Cadle, and W. A. Sedlack, 1980: Vertical mass- and trace constituent transports in the vicinity of jet streams. *Arch. Meteor. Geoph. Biokl.*, **28B**, 193–206, https://doi.org/10.1007/BF02245351.

Sinnhuber, B.-M., and S. Meul, 2015: Simulating the impact of emissions of brominated very short lived substances on past stratospheric ozone trends. *Geophys. Res. Lett.*, **42**, 2449–2456, https://doi.org/10.1002/2014GL062975.

——, and Coauthors, 2000: Large loss of total ozone during the Arctic winter of 1999/2000. *Geophys. Res. Lett.*, **27**, 3473–3476, https://doi.org/10.1029/2000GL011772.

——, M. Weber, A. Amankwah, and J. P. Burrows, 2003: Total ozone during the unusual Antarctic winter of 2002. *Geophys. Res. Lett.*, **30**, 1580, https://doi.org/10.1029/2002GL016798.

——, G. Stiller, R. Ruhnke, T. von Clarmann, S. Kellmann, and J. Aschmann, 2011: Arctic winter 2010/2011 at the brink of an ozone hole. *Geophys. Res. Lett.*, **38**, L24814, https://doi.org/10.1029/2011GL049784.

Smith, K. L., and L. M. Polvani, 2014: The surface impacts of Arctic stratospheric ozone anomalies. *Environ. Res. Lett.*, **9**, 074015, https://doi.org/10.1088/1748-9326/9/7/074015.

Solomon, S., J. Haskins, D. J. Ivy, and F. Min, 2014: Fundamental differences between Arctic and Antarctic ozone depletion. *Proc. Natl. Acad. Sci. USA*, **111**, 6220–6225, https://doi.org/10.1073/pnas.1319307111.

Spichtinger, P., and K. M. Gierens, 2009: Modelling of cirrus clouds—Part 1a: Model description and validation. *Atmos. Chem. Phys.*, **9**, 685–706, https://doi.org/10.5194/acp-9-685-2009.

Stratmann, G., and Coauthors, 2016: NO and NO_y in the upper troposphere: Nine years of CARIBIC measurements onboard a passenger aircraft. *Atmos. Environ.*, **133**, 93–111, https://doi.org/10.1016/j.atmosenv.2016.02.035.

Thompson, D. W. J., S. Solomon, P. J. Kushner, M. H. England, K. M. Grise, and D. J. Karoly, 2011: Signatures of the Antarctic ozone hole in Southern Hemisphere surface climate change. *Nat. Geosci.*, **4**, 741–749, https://doi.org/10.1038/ngeo1296.

Ungermann, J., and Coauthors, 2011: A 3-D tomographic retrieval approach with advection compensation for the air-borne limb-imager GLORIA. *Atmos. Meas. Tech.*, **4**, 2509–2529, https://doi.org/10.5194/amt-4-2509-2011.

Voigt, C., and Coauthors, 2000a: Nitric Acid Trihydrate (NAT) in polar stratospheric clouds. *Science*, **290**, 1756–1758, https://doi.org/10.1126/science.290.5497.1756.

——, and Coauthors, 2000b: Non-equilibrium compositions of liquid polar stratospheric clouds in gravity waves. *Geophys. Res. Lett.*, **27**, 3873–3876, https://doi.org/10.1029/2000GL012168.

——, and Coauthors, 2005: Nitric Acid Trihydrate (NAT) formation at low NAT supersaturation in polar stratospheric clouds. *Atmos. Chem. Phys.*, **5**, 11 371–11 380, https://doi.org/10.5194/acp-5-1371-2005.

——, and Coauthors, 2014: Evolution of CO_2, SO_2, HCl, and HNO_3 in the volcanic plumes from Etna. *Geophys. Res. Lett.*, **41**, 2196–2203, https://doi.org/10.1002/2013GL058974.

——, and Coauthors, 2017: ML-CIRRUS: The airborne experiment on natural cirrus and contrail cirrus with the high-altitude long-range research aircraft HALO. *Bull. Amer. Meteor. Soc.*, **98**, 271–288, https://doi.org/10.1175/BAMS-D-15-00213.1.

——, and Coauthors, 2018: Widespread polar stratospheric ice clouds in the 2015–2016 Arctic winter – implications for ice nucleation. *Atmos. Chem. Phys.*, **18**, 15 623–15 641, https://doi.org/10.5194/acp-18-15623-2018.

von Hobe, M., and Coauthors, 2013: Reconciliation of essential process parameters for an enhanced predictability of Arctic stratospheric ozone loss and its climate interactions (RECONCILE): Activities and results. *Atmos. Chem. Phys.*, **13**, 9233–9268, https://doi.org/10.5194/acp-13-9233-2013.

Wagner, J., and Coauthors, 2017: Observed versus simulated mountain waves over Scandinavia – Improvement of vertical winds, energy and momentum fluxes by enhanced model resolution? *Atmos. Chem. Phys.*, **17**, 4031–4052, https://doi.org/10.5194/acp-17-4031-2017.

Waibel, A. E., and Coauthors, 1999: Arctic ozone loss due to denitrification. *Science*, **283**, 2064–2069, https://doi.org/10.1126/science.283.5410.2064.

Weber, M., S. Dhomse, F. Wittrock, A. Richter, B.-M. Sinnhuber, and J. P. Burrows, 2003: Dynamical control of NH and SH winter/spring total ozone from GOME observations 1995–2002. *Geophys. Res. Lett.*, **30**, 1583, https://doi.org/10.1029/2002GL016799.

Werner, A., C. M. Volk, E. V. Ivanova, T. Wetter, C. Schiller, H. Schlager, and P. Konopka, 2010: Quantifying transport into the Arctic lowermost stratosphere. *Atmos. Chem. Phys,*. **10**, 11 623–11 639, https://doi.org/10.5194/acp-10-11623-2010.

Wetzel, G., and Coauthors, 2015: Partitioning and budget of inorganic and organic chlorine species observed by MIPAS-B and TELIS in the Arctic in March 2011. *Atmos. Chem. Phys.*, **15**, 8065–8076, https://doi.org/10.5194/acp-15-8065-2015.

Wirth, M., A. Fix, P. Mahnke, H. Schwarzer, F. Schrandt, and G. Ehret, 2009: The airborne multi-wavelength water vapor differential absorption lidar WALES: System design and performance. *Appl. Phys.*, **96B**, 201, https://doi.org/10.1007/s00340-009-3365-7.

WMO, 2018: Scientific assessment of ozone depletion: 2018. WMO Global Ozone Research and Monitoring Project Rep. 58, 590 pp., www.esrl.noaa.gov/csd/assessments/ozone/2018/.

Woiwode, W., and Coauhtors, 2018: Mesoscale fine structure of a tropopause fold over mountains. *Atmos. Chem. Phys.*, **18**, 15 643–15 667, https://doi.org/10.5194/acp-18-15643-2018.

Zahn, A., J. Weppner, H. Widmann, K. Schlote-Holubek, B. Burger, T. Kühner, and H. Franke, 2012: A fast and precise chemiluminescence ozone detector for eddy flux and airborne application. *Atmos. Meas. Tech.*, **5**, 363–375, https://doi.org/10.5194/amt-5-363-2012.

Ziereis, H., H. Schlager, H. Fischer, C. Feigl, P. Hoor, R. Marquardt, and V. Wagner, 2000: Aircraft measurements of tracer correlations in the Arctic subvorter region during the Polar Stratospheric Aerosol Experiment (POLSTAR). *J. Geophys. Res.*, **105**, 24 305–24 313, https://doi.org/10.1029/2000JD900288.

——, and Coauthors, 2004: Uptake of reactive nitrogen on cirrus cloud particles during INCA. *Geophys. Res. Lett.*, **31**, L05115, https://doi.org/10.1029/2003GL018794.

Zöger, M., and Coauthors, 1999: Fast in situ stratospheric hygrometers: A new family of balloon-borne and airborne Lyman alpha photofragment fluorescence hygrometers. *J. Geophys. Res.*, **104**, 1807–1816, https://doi.org/10.1029/1998JD100025.